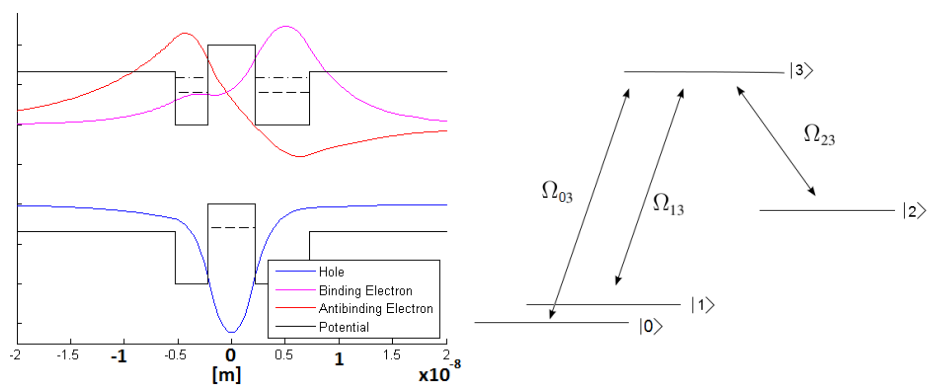# DTU

Danmarks Tekniske Universitet

DTU Photonics
B.Sc. Thesis
June 25, 2015

Optical Quantum Gates in Nanowires

Written by:
Nicklas Larsen s123518
Jakob Ravnskjær s123826

Supervisors:
Nika Akopian
Niels Gregersen
Dara McCutcheon

Abstract

The primary goal of this project was to achieve a higher understanding of optical quantum gating in nanowires. In the project a quantum mechanical investigation of the STIRAP method was made in order to understand how the optical gating can be improved. In order to improve the STIRAP process we found through the rabi frequencies that the transition dipole moments of the system had to be large to optimize adiabatic transition. In order to calculate the dipole moments a full calculation of the single particle wavefunctions in the envelope approximation has been made for the nanowires. In order to optimize the dipole moments, we adjusted the potential landscape and noted several different tendencies. These include confinement of electrons in specific dots, the behaviour of the overlap, and energies. Finally we seek out improvements to our calculations by including the coulomb interaction and the charged exciton wavefunction. This was found too time consuming and was not realizable within a reasonable time period.

Contents

Chapter 1

Introduction

Moore's law states that the number of transistors in a computer has to double every 18 months, and by extension the processing speed goes up. This means that problems can be solved quicker and more efficiently with computers of today.

There are certain problems that scales faster in computation time for increasing complexity. Some problems will not be efficiently solvable before Moore's law reaches its physical limitation. Quantum computers and related algorithms can however decrease the computation time scaling with respect to problem complexity and make the problems efficiently solvable. An example hereof is Shor's Algorithm which is used to factorize large prime numbers fast and efficiently[1].

The quantum computer is already described in the bra ket formalism by quantum mechanics, however the physical implementation is still in its infancy. David DiVincenzo set up in his paper 5 requirements for the physical implementation of the quantum computer [2]. The system has to have well defined qubits that are initializable, longer coherence time than gating time, and for a universal set of quantum gates to exist, and the ability to measure the qubits.

We shall use electron spins as qubits in this project. The gating is realised with the STIRAP method which, as will be shown, is a very effective way of coherent population transfer. Afterwards system parameters will be investigatied in order to show how the system behaves, and hereby qualitatively improve the gating process. Finally we suggest methods for improving the model of the system in order to reach more quantitatively correct results which is left for future investigation.

1.1 Qubits

As in conventional computers, quantum computers also operate on a binary basis. The quantum equivalent of the bit is called the qubit, and contains two distinct orthogonal states - conventionally labelled $|0\rangle$ and $|1\rangle$. The idea of a qubit is general, and is independent on the physical system used to implement the qubit. A qubit differs from the classical bit by the ability for it to take a superposition between the two orthogonal states.

The implementation of a qubit investigated in this project is electron spins located

in a quantum dot, with a second auxillary quantum dot located close by to use for gating. The spins constitute the qubit basis, $\{|0\rangle, |1\rangle\}$ for spin down and for spin up respectively.

The dots are created by growing nanowires of the same material in different crystal structures to alter the potential landscape. The nanowires are made from InP and are grown in wurzite (WZ) and zincblende (ZB) structures in the z direction as shown on figure 1.1. The band gaps used are from [3].
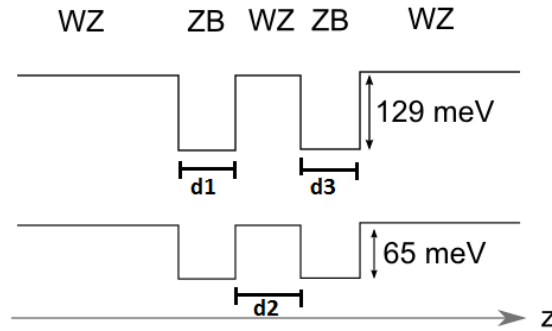
Figure 1.1: The potential landscape in the z direction of the nanowires used to implement quantum gating in this project

We also need to be able to measure the spin state which our electron is in at a given point after the gating process. There are a couple of methods in how to do this. One method is to apply an electric field to split the energy of the spin up and spin down of the electron by the corresponding Zeeman energy. The field needs to be tuned in such way that one spin the electron will leave the dot and with the opposite spin it will stay. A Quantum Point Contact (QPC), can then be used to measure the charge of the dot, and hereby determine the spin of the electron. [4]

1.2   Gating

In order to make a gate, it has to be possible to coherently transfer population from one of the spin states to the other. As will be shown in the following sections it is advantageous to keep the sizes of the dots different in order to localise the qubit basis in one of the dots and keep the other one empty until gating[5]. A robust population transfer method is prefered, such that the population transfer happens as efficiently as possible.

Gating in quantum information is divided into two branches, conditional and unconditional gating, for multiple and single qubit state changes respectively. We shall seek to treat the unconditional gating thoroughly and leave conditional gating to only be briefly mentioned and discussed. From here on gating refers to unconditional gating unless otherwise specified.

In order to make gating on the system, population should be transferred from one eigenstate in a (possible) superposition to another. This will be done in the same way as described in [5], using an (approximate) lambda level system, where the spin

up and down has been combined as one energy in figure 1.2. The scheme is then to pick out, depending on the polarisation of light, a chosen spin eigenstate population, transfer it to the optically inaccessible state $|2\rangle$ (wavefunction in second dot) using state $|3\rangle$ (charged exciton) as an extra auxillary state that allows optical coupling, and perform the rotation into the other state on the way back.

The theory behind these transitions will be discussed in detail in the following section. We start off by investigating the theory behind raman transitions in order to introduce the rotating wave approximation and rabi frequencies in a simple way. These are used in the STIRAP process which we shall se is superior to doing raman transitions.
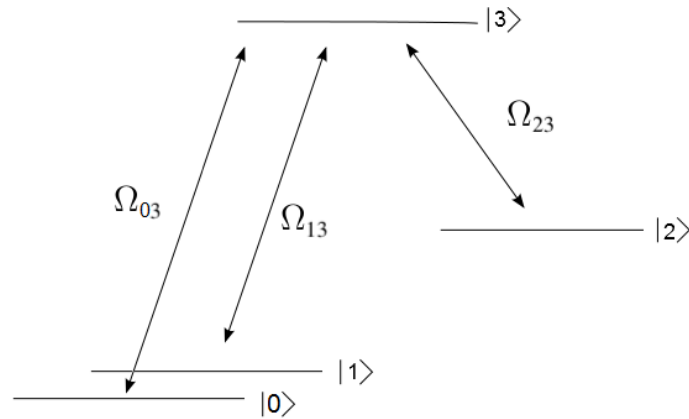
Figure 1.2: The lambda level structure

1.2.1 Raman transitions

In order for the population of the energy eigenstates to change, the hamiltonian of the system has to be perturbed. This is conventionally done by applying an electric field with a laser pulse [6]. The theory behind this time dependent hamiltonian is that of time dependent phenomena and induced emission and absorbtion as described in [7]. Transferring population from one state to an optically inaccessible state through a third state is the method of raman transitions, from which some of the terminologi will also be applied. The hamiltonian of the monochromatic laser light is:

$$\hat{H}_{Laser} = -q\boldsymbol{x} \cdot \boldsymbol{E}_0 \frac{1}{2} \left(\exp\left(-i\omega t\right) + \exp\left(i\omega t\right) \right) \tag{1.1}$$

with $\boldsymbol{E}_0$ being the electric field vector, taken to be a slowly varying pulse such that it can be thought of as constant in the following treatment of the problem. This is under the electric dipole approximation[1], where the spatial variation of the field over the size of the system is negligible and the magnetic field can be neglected, and thus the hamiltonian is independent of magnetic effects and the electric field is independent of spatial coordinates.

---

[1]The electric dipole approximation is mathematically done by approximating $\exp\left(i\boldsymbol{k} \cdot \boldsymbol{r}\right) = 1 + \boldsymbol{k} \cdot \boldsymbol{r} + \dots$ by the first term, 1.

Now a general time dependent state vector for the system can be expanded in the eigenvector basis for the initial hamiltonian.

$$|\Psi(t)\rangle = \sum_n c_n(t) \exp\left(-iE_n t/\hbar\right)|n\rangle \tag{1.2}$$

Where the c_n's are expansion coefficients with the requirement $\sum_n |c_n(t)|^2 = 1$. Inserting this state into the time dependent Schrödinger equation and simplifying, one obtains a generel equation for the expansion coefficients of a state vector in time dependent perturbation theory.

$$\dot{c}_m(t) = -\frac{i}{\hbar}\sum_n \langle m| \hat{H}_{Laser} |n\rangle \exp\left(i\frac{E_m - E_n}{\hbar}t\right)c_n(t) \tag{1.3}$$

$$= \frac{i}{2\hbar}\sum_n q \langle m| \boldsymbol{E}_0\boldsymbol{r} |n\rangle \left(\exp\left(-i\omega t\right) + \exp\left(i\omega t\right)\right)\exp\left(i\omega_{mn}t\right)c_n(t) \tag{1.4}$$

$$= \frac{i}{2\hbar}\sum_n q \langle m| \boldsymbol{E}_0\boldsymbol{r} |n\rangle \left(\exp\left(-i(\omega - \omega_{mn})t\right) + \exp\left(i\left(\omega + \omega_{mn}\right)t\right)\right)c_n(t) \tag{1.5}$$

Where the dot represents differentiation with respect to time, and ω_{mn} is the transsition frequency between the two states, m and n, defined by $\omega_{mn} = \frac{E_m - E_n}{\hbar}$.

If the frequency of the laser light applied closely corresponds to that of the energy differences between two states of the quantum dot, these two states become very dominant in the sum in equation (1.5) when calculating c_m. The reason for this is that only one term in the sum is varying slowly over timescales longer than optical waves (femtosecond), and as such does not "average out". The rest of the terms can be neglected and we are left with:

$$\dot{c}_m(t) = \frac{i}{2\hbar}q \langle m| \boldsymbol{E}_0\boldsymbol{r} |n\rangle \exp\left(-i(\omega - \omega_{mn})t\right)c_n(t) \tag{1.6}$$

This is the rotating wave approximation. The inner product $q \langle m| \boldsymbol{E}_0\boldsymbol{r} |n\rangle$ is refered to as a dipole matrix element. This also suggests that the system is essentially a two level system when considering the dynamics. For the sake of simplicity, and without loss of generality the system will now be treated as such.

The lambda level structure can be thought of as two individual two level systems where the transitions are determined by the choice of light frequency - see figure 1.2. The only effect of the two level consideration is that the hilbert space is spanned completely by the two state vectors of the interacting levels. These will be labled, g and e, for ground and excited state respectively. Assuming no detuning between the laser and the nanowires the exponential reduces to a factor of 1. This leaves us with a coupled set of differential equations:

$$\dot{c}_g = \frac{i}{2\hbar}q \langle g| \boldsymbol{E}_0\boldsymbol{r} |e\rangle c_e(t) \tag{1.7}$$

$$\dot{c}_e = \frac{i}{2\hbar}q \langle e| \boldsymbol{E}_0\boldsymbol{r} |g\rangle c_g(t) \tag{1.8}$$

This set of differential equations have the solutions under the initial condition that the population is completely in the ground state and keeping the norm squared sum of the coefficients to unity. The dipole moments are taken to be real:[8]

$$c_e(t) = i \sin\left(\Omega t/2\right) \tag{1.9}$$

$$c_g(t) = \cos\left(\Omega t/2\right) \tag{1.10}$$

Where $\Omega = q \langle e| \boldsymbol{E}_0 \boldsymbol{r} |g\rangle / \hbar$ is the rabi frequency. From this the probability of the state vector being completely in the excited state will be:

$$|c_e(t)|^2 = \sin\left(\Omega t/2\right)^2 \tag{1.11}$$

When the time duration of the pulse exactly corresponds to π/Ω the transition probability reaches its maximum for perfect resonance/no detuning. This is commonly refered to as a Pi-Pulse. These Pi-Pulses can in principle be used to transfer population between two states. To make a complete transfer from state $|1\rangle$ (or $|0\rangle$) to $|2\rangle$ in figure 1.2 one would first with a 1-3 Pi pulse, referred to as a pump pulse in stimulated raman scattering, excite all the population initially in $|1\rangle$ to $|3\rangle$, and then afterwards transfering from $|3\rangle$ to $|2\rangle$ with a so called stokes pulse.

The strong dependence on system parameters and the requirement that the pulse has to be an exact pi-pulse makes it very difficult to realise in the quantum dots. Furthermore if the excited state suffers from radiative decay the coherence of the qubit will be lost, as is the case for this lambda level system as described earlier, where the state accessible by laser light is the charged exciton state, in which the electron and hole will recombine under emission of radiation.

1.2.2   STIRAP

Another approach to this problem is the stimulated raman adiabatic passage (STIRAP). This approach is somewhat similar to the raman transitions, however the time dependence of the electric field vector now becomes important, and thus also the time dependence of the rabi frequencies. It will also show that the stokes pulse should counterintuitively be applied first and then the pump pulse afterwards[9]. This method is not nearly as dependent on the experimental parameters and as such is much more robust, in that it has a plateau of optimum delay between the pump and stokes pulses as seen in [6] and [10].

The hamiltonian of the 3 level system in figure 1.2 is described by [11],[12].

$$\hat{H} = -\frac{1}{2}\hbar \begin{bmatrix} 0 & \Omega_1(t) & 0 \\ \Omega_1(t) & 2\Delta(t) & \Omega_2(t) \\ 0 & \Omega_2(t) & 0 \end{bmatrix} \tag{1.12}$$

For which one of the eigenstates is a so called dark state, since it does not contain the radiative state (the exciton) where coherence can be lost. The dark state is:

$$|u_1(t)\rangle = \cos\left(\theta(t)\right)|1\rangle - \sin\left(\theta(t)\right)|2\rangle \tag{1.13}$$

with $\tan\theta(t) = \frac{\Omega_1(t)}{\Omega_2(t)}$. It is noted that for complete transfer from state $|1\rangle$ to $|2\rangle$ the

rabi frequencies need to fulfill the relations [11]

$$\frac{\Omega_1(t)}{\Omega_2(t)} \to 0, \quad \text{for } t \to -\infty \tag{1.14}$$

$$\frac{\Omega_2(t)}{\Omega_1(t)} \to 0, \quad \text{for } t \to \infty \tag{1.15}$$

This shows that initially there is no pump pulse connecting state $|1\rangle$ and $|3\rangle$, and in the final situation no stokes pulse connecting state $|3\rangle$ and $|2\rangle$. However these pulses should overlap [6], [11]. Selecting between the spin states $|0\rangle$ or $|1\rangle$ - very close in energy - is done by the choice of polarisation of the light, with polarisation vector in x (y) corresponds to adressing state $|0\rangle$ ($|1\rangle$) in the pump pulse[5] [13]. The Stokes pulse is x-polarised. Performing a second reversed Stirap process, where the pump pulse now can be chosen at any polarisation allows for spin state rotation.

The rabi frequencies will in general be denoted $\Omega_0(t) = \Omega(t)\cos(\chi)$ and $\Omega_1 = \Omega(t)\exp(i\eta)\sin(\chi)$ for spin down and spin up respectively, where χ and η are phase-factors. The envelope $\Omega(t)$ is the same in both cases since the wavefunctions are the same. As an example of initialization of the qubit consider this being in the unknown initial state $\alpha|0\rangle + \beta|1\rangle$, which is desired to be completely in the $|0\rangle$ state. In order to transfer the unwanted population from $|1\rangle$ the choice of phase factors should simply be $\chi = \pi/2, \eta = 0$. If the choice of parameters on the reversed stirap are $\chi = 0$ and $\eta = 0$ the final state will be: $|0\rangle$ and thus the qubit state is initialized. Being able to initialize qubits to a fiducial state is one of the requirements set forth by [2].

A gate should be able to make a true rotation of an unknown input state around a chosen axis. This is done by applying two overlapping pump pulses with different rabi frequencies, to adress both the $|0\rangle$ and $|1\rangle$ states on the first stirap process, and chosing a phase shift, δ, on the stokes pulse on the way back. As described by [14] the final state after such a process is $|\psi_f\rangle = \exp(-i\delta/2)\hat{R}_n(\delta)|i\rangle$, with $\hat{R}_n$ being a rotation matrix around an axis specified by n, and $|i\rangle$ being an arbitrary input state. As such all rotations can be performed on arbitrary input states, and this constitutes our single particle gate. The extra phase factor, $\exp(-i\delta/2)$, is for single qubit gates a global phase and can be forgotten, however considering a system of multiple qubits it has to be included in the algorithms.

The conditional gate is implemented by letting two sets of quantum dot structures interact with coulomb interaction. First the control qubit is transferred to $|2\rangle$, which changes the transition frequencies for the target qubit. Because of this the taget qubit will be rotated dependent on the position of the first qubit [5]. Thus a universal set of gates has been found in accordance with the requirements from [2].

In order for the system to carry the population from $|1\rangle$ to $|2\rangle$ adiabatically, i.e. without the radiative losses from $|3\rangle$ the rabi frequencies need to be large [6]. This can either be done by increasing the intensity of the incoming light or by increasing the dipole moment. Increasing the intensity is an external parameter that does not rely on the system, and is not really interesting in the engineering of the nanowires. Furthermore the larger the intensity the more nanowires will heat up and in the ex-

treme case eventually melt. This tells us that the nanowires need to be engineered in such a way that the dipolemoments are as large as possible. Thus we seek to maximize the dipole moments which will be the primary focus of this thesis. In order to optimize the dipole moments, we must first determine the wavefunctions/eigenstates of the system. The following section will deal with this, and afterwards we shall move on to the optimization.

Chapter 2

Wavefunctions

The following section deals with approximations to the system and solving the Schrödinger equation in the noninteracting particle picture (no Coulomb interaction) for the electron and hole under these approximations. The most important part of the wavefunction for transitions is the z-direction, but suggestions for the radial part are also proposed. The hole wavefunction is in the single particle picture not confined by the potential, but needs coulomb interaction to stay in the double dot structure. Furthermore due to the conditional gate being based on electron wavefunction localization in the z direction, the localization will be investigated.

2.1 Envelope approximation

The envelope approximation, is a very useful approximation when looking at wave functions propagating through a periodic potential which occurs in solids. It is an approximation in which it is assumed that the envelope of a wave function varies in time and space much slower, compared to the period of the wave function. All the wave functions which are calculated in this report and the potential landscape in figure 1.1 are based off of this approximation.

It is useful to use the envelope approximation, since the equations needed to be solved usually are easier, since the order of partial derivatives is reduced. The envelope approximation comes directly from Bloch's theorem which states that a wave through a periodic potential can be described as

$$\psi(x) = u(x)F(x) \tag{2.1}$$

Where $u(x)$ is called the Bloch function and is an oscillating periodic function, with periodicity that is equal to the crystal lattice i.e. $u(x + a) = u(x)$ where a is the lattice parameter. $F(x)$ is the envelope function, that describes the outskirts of the function $u(x)$. For a slowly varying envelope function relative to the Bloch function $u(x)$, the envelope describes the most important properties of the wave function i.e. the energy levels and overlap. The envelope functions holds the most important features of the actual wave function[15]. The wavefunctions are calculated based on this approximation.

2.1.1 Electron wave function

The electron wavefunction is calculated from the non interacting hamiltonian in the envelope approximation, where the potential in the z-direction and transverse direction seperate:

$$\hat{H}_0 = -\frac{\hbar^2}{2m_\text{eff}}\nabla^2 + V_{DW}(z) + V_T(x,y) \tag{2.2}$$

With the potential in z being the double well structure shown in figure 1.1. The solutions are, using the method of separation of variables, seperated wavefunctions in the z and transverse direction. The wavefunction in the z direction is a piecewise function defined differently in each WZ/ZB part, with energies solved analytically. The wavefunction for the ground state and first excited state for different seperation widths of the well is plotted in figure 2.1, with equal well widths as in [16]. The two states are commonly refered to as binding and antibinding hybridizations of the dots [17]. The binding wavefunction is related to $|0\rangle$, $|1\rangle$ and the antibinding to $|2\rangle$ in the lambda level structure (figure 1.2). The energy of binding and antibinding

Seperation distance 1.2nm

Seperation distance 2.8nm
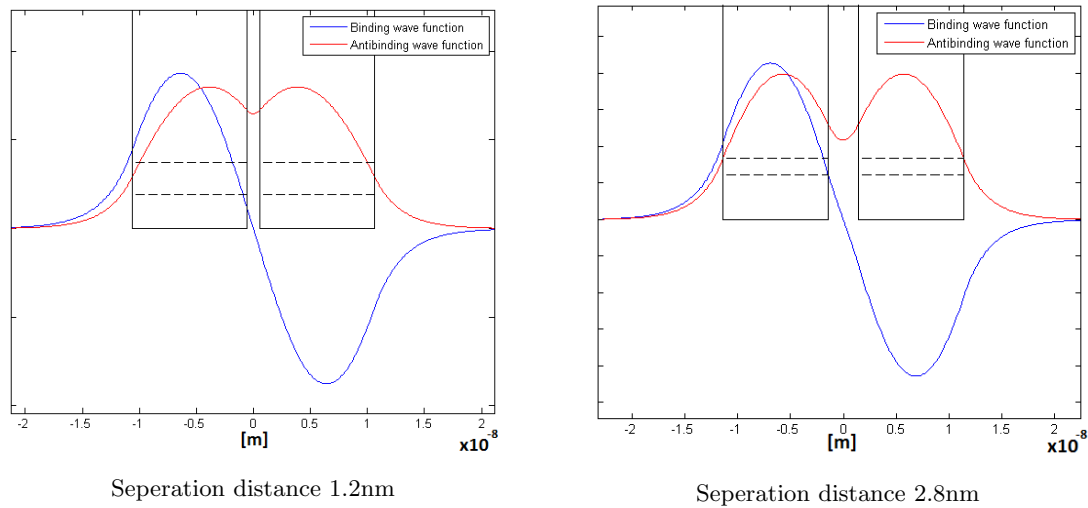
Figure 2.1: The wavefunctions in z direction for the ground state and first excited state for different well seperation distances. Well widths are 10nm. The dashed lines correspond to the energies of the wavefunctions with the binding being the lowest and the antibinding the highest.

wavefunctions are plotted in figure 2.2. As the separation width increases the energies approach eachother.

The transverse part of the wavefunction is calculated in two different ways, inspired by the confinement potentials described in [18], with either a parabolic confinement or a 2d spherical infinite quantum well potential with zero wavefunction boundary conditions in the radius of the wire. The parabolic potential is often used in relation with self assembled quantum dots, but for the nanowires we suspect the potential to be approximately flat throughout the transverse part of the nanowire, due to the well defined geometry and potential. First off is the parabolic potential which is modelled as $V(r) = \frac{1}{2}m\omega^2 r^2$. The solution to the Schrödinger equation in the transverse direction becomes the Fock-Darwin states with the analytical expression

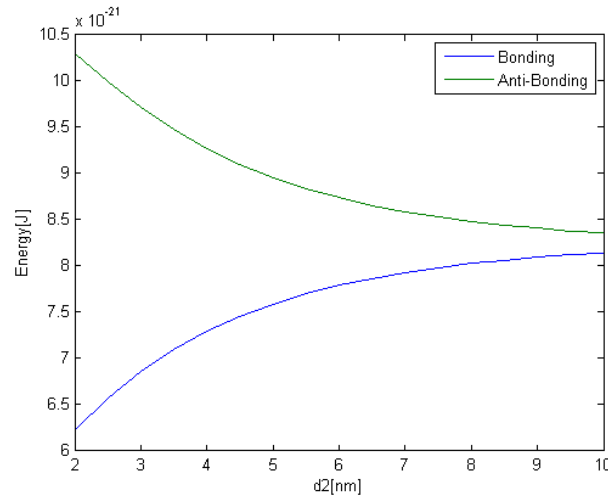*Figure 2.2:* The energy of the binding and antibinding wavefunction as a function of the electron well separation distance $d2$

for the wavefunction: $\psi_R(r, \theta) = r^m \exp\left(-r^2/2\right) L_m^k\left(r^2\right) \exp\left(im\theta\right)$, with m and k as solution parameters (quantum numbers). The energy in the transverse direction is $E_T = (2k + m + 1)\hbar\omega$. The real part of the wavefunctions are plotted for $k, m = 0$ and $k, m = 1$ in figure 2.3.

With an infinite well in the transverse direction the solution is given by the bessel

$k, m = 0$ $k, m = 1$

Figure 2.3: The real part of the wavefunctions in the transverse direction with a parabolic potential for different values of the quantum numbers m and k.

function: $\psi_T(r, \theta) = A J_n(\lambda r) \exp\left(in\theta\right)$ with λ and n being solution parameters (quantum numbers). The energy is found from the zeros of the bessel function and the radius of the wire. This solution is expected to bear the closest resemblance with the real wavefunctions in nanowires.

The transverse part of the wavefunction is not used to calculate the dipolemoment since it will not change from the ground state and thus the overlaps with eachother is unity. The calculations of the Schrödinger equation are carried out in depth in appendix A.1.
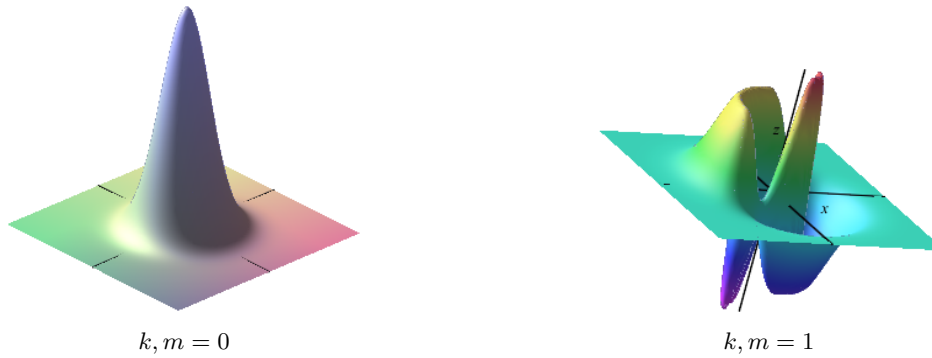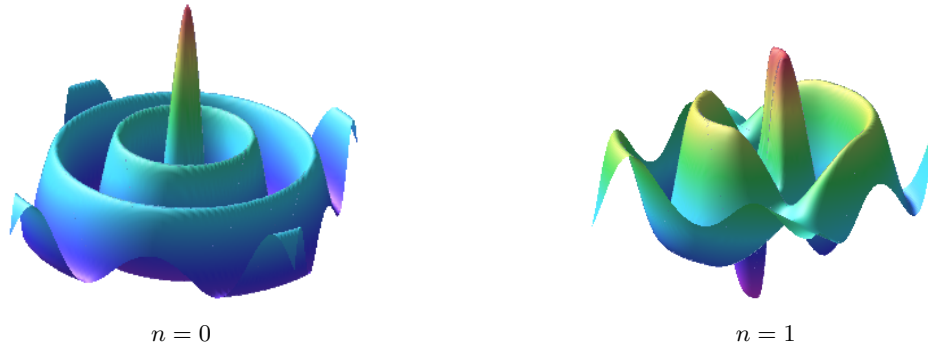
$n = 0$ $n = 1$

Figure 2.4: The real part of the wavefunctions in the transverse direction with a quantum well potential for different values of the quantum number n. Lambda is in this case arbitray since the view fiels is also are arbitray. The plot should be cut off in the radius equal to the radius of the nanowire.

2.1.2 Hole wavefunction

The single particle wavefunctions for the hole should be calculated from the valence band in figure 1.1. This however leads to a delocalised wavefunction since the hole can tunnel out of the barriers confining it. The only thing keeping the hole in the dot structure is the Coulomb interaction with the electron which is not included.

In order to get bound single particle wavefunctions for the hole a superlattice is introduced after the electron wells, such that the potential landscape is as shown on figure 2.5. This superlattice is essentially WZ-ZB layers alternating on a very small scale such that the potential averages to a factor, called $g \in [0 \ 1]$, times the original band offsets. The hole wavefunction is then solved in the same way as the electron wavefunctions above. From now on the wavefunctions will all be calculated
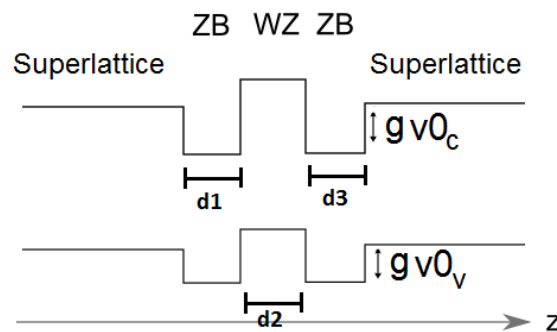
Figure 2.5: The potential landscape in z-direction with the super lattice in the end of the nanowires to ensure confinement of the hole single particle wavefunction.

including this superlattice to ensure hole confinement.

2.1.3 Ensuring spatial confinement in the wells

As discussed in section 1.2 the conditional gate requires definite localisation in the wells for the wavefunctions in the states $|0\rangle, |1\rangle$ (same wavefunction) and state $|2\rangle$. The eigenfunctions of the hamiltonian in figure 2.1 unfortunately do not satisfy this

requirement. The system can be prepared in superposition states which are not eigenstates of the hamiltonian but ensures confinement in the dots. The superposition states are $\psi_+ = \frac{1}{\sqrt{2}} (|B\rangle + |A\rangle)$ and $\psi_- = \frac{1}{\sqrt{2}} (|B\rangle - |A\rangle)$, where B and A refers to the binding and antibinding eigenfunctions, respectively. As seen on figure 2.6

(a) Separation distance 1.2nm

(b) Separation distance 2.8nm

Figure 2.6: Binding minus antibinding and binding plus antibinding wave function, with wells of equal size (10nm). Superlattice parameter is set to 0.6. The probability of being in the desired well is 0.88 and 0.90 for the small and large seperation respectively. The probability is 0.027 and 0.007 in the opposite well. ($\psi_\pm$ is symmetric so the possibilities are the same)

the superposition state is really confined in each well, with ψ_+ being on the left and ψ_- being on the right. However being in a superposition 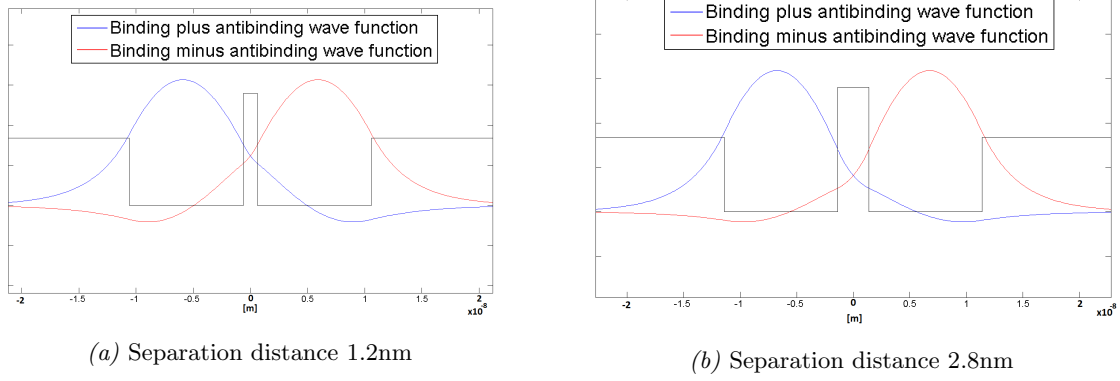state means that under time evolution the eigenfunction basis states will not just obtain an irrelevant global phase, but a phase difference with respect to eachother. This means that the superposition state changes position over time.

When the phase difference reaches π the electron will go from being in one dot to the other, i.e. $\psi_+ \rightarrow \psi_-$. The transition time of this "tunneling" can be calculated from the unitary time evolution operator for time independent hamiltonians, $\hat{U}(\Delta t) = \exp\left(-i\Delta t \hat{H}/\hbar\right)$, on the state. This gives

$$T = \frac{\pi\hbar}{E_A - E_B} \tag{2.3}$$

Where T is the transition time, E_B and E_A are the binding and anti-binding energy respectively. It shows the difference in energy needs to be as small as possible in order to increase the transition time, T. As seen on figure 2.7a the transition time increases as $d2$ increases. The transition time for the chosen parameter values is in the order of picoseconds. Picoseconds are too quick for the system to have well defined temporal confinement in the dots and thus the gating will not work. This could suggest that a system with a large $d2$ and $d1 = d3$ would be good, since a measurement will always be correct on the system. But since the overlap also needs to be optimized, this has to be checked as well.

On figure 2.7b we see a tendency that shows a decrease in the overlap as $d2$ increases, and since we wish to optimize the overlap so the transition between levels can be done faster and still be adiabatic, just increasing $d2$ is not a valid option.

(a) Transistion time as function of d2, with constant d1=d3=5nm
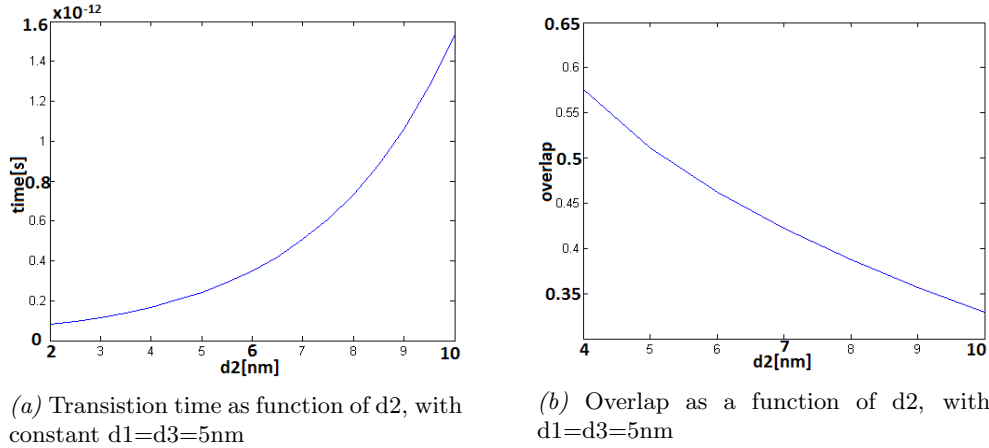

(b) Overlap as a function of d2, with d1=d3=5nm

Figure 2.7: Concers for the superposition state

Furthermore the system is not in an energy eigenstate and thus cannot be adressed effectively by the laser pulses in the STIRAP process.

One way of engineering the potential landscape is with inequal widths of the wells. This ensures both confinement in either dot and seperated energy levels of the two orthogonal wavefunctions. This is plotted in figure 2.8.

(a) $d1 = 10\,\text{nm}, d2 = 1.2\,\text{nm}, d3 = 8\,\text{nm}$. The probability of being in the leftmost dot is 0.62 and 0.32 for the binding and antibinding respectively. The rightmost dot 0.29 is 0.54 for B and A respectively.

(b) $d1 = 10\,\text{nm}, d2 = 2.8\,\text{nm}, d3 = 8\,\text{nm}$. The probability of being in the leftmost dot is 0.73 and 0.18 for the binding and antibinding respectively. The rightmost dot 0.15 is 0.69 for B and A respectively.
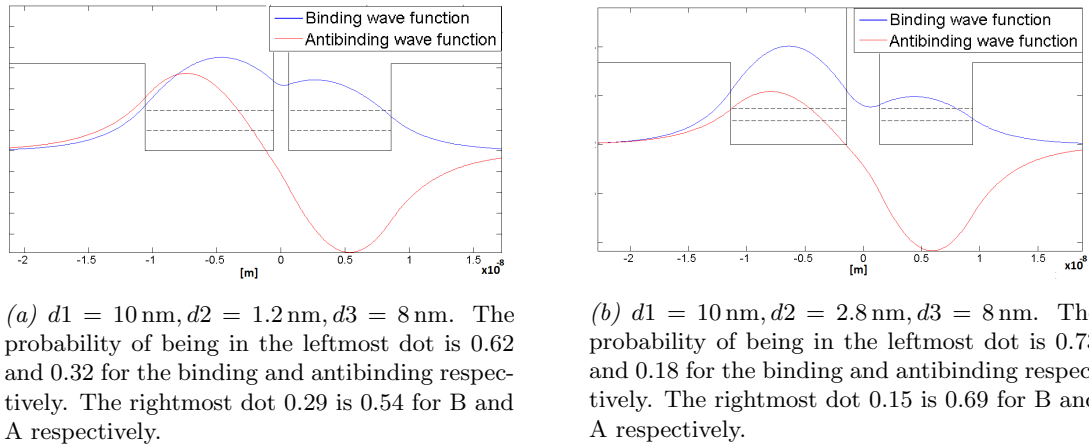
Figure 2.8: Binding and antibinding with different well widths. Superlattice parameter is 0.6.

Figure 2.8 shows that the binding and anti binding function is somewhat confined in each dot, and the confinement increases with increasing separation distance. Chosing eigenstates also gets rid of the transmission time problem, since eigenstates do not change in time.

Now the single particle wavefunctions of the system has been determined. The confinement of the wavefunctions has been ensured, without introducing time dependent phenomena since they are eigenstates. Thus the qubits are well defined and do not lose coherence too quickly. This is one of the requirements of [2].

Chapter 3

Potential landscape optimization

Now the dipole moments are calculated. As calculated in section 1.2.1 the dipole moments are given by the matrix element $\langle m | q\boldsymbol{E}_0 \boldsymbol{r} | n \rangle$. The wavefunctions are given by a bloch wave and an envelope as shown in section 2.1. The matrix element splits up into bloch elements and envelope, with the bloch wavefunctions carrying the spatial dependence - these are typically experimentally determined. This is shown in appendix A.4. The dipole moment that we want to optimize becomes $\langle e_{\text{envelope}} | h_{\text{envelope}} \rangle$ [19]. The overlap of the envelopes are optimized in the z direction. The radial parts of the wavefunctions will be unchanged in the lambda level structure on figure 1.2, and as thus the overlap will only be determined by the z-direction overlap since the radial part overlap evaluates to 1.

3.1 Single well approximation

In order to start the calculations, the wells for the electrons are conceptually placed infinitely far away from eachother, and are then moved together. The approximation is then that the wavefunctions in the wells do not change or in any way feel the effect the other well. This approximation is conceptually good for large separation distances, and will qualitatively show some of the tendencies of the system. The z dependence of the wavefunctions for both the electrons and the hole are calculated for different values of the parameter that is investigated, $\left| \psi_{z_1}^e \right\rangle, \left| \psi_{z_2}^e \right\rangle, \left| \psi_z^h \right\rangle$ and the overlaps, $\int \psi_{z_n}^e \psi_z^h dz$, between the hole and the electrons are calculated and plotted. We start off with only investigating one electron well with the hole, to focus on isolated tendencies of the hole and electron well width parameters.

3.1.1 Electron well widths

First the width of the wells for the electrons are investigated. The potential landscape, wavefunctions and energies for a given value of $d1$ are seen plotted on figure 3.1a. The overlaps of the first and second electron with the hole as a function of $d1$ are seen on figure 3.1b The overlap seems to take a maximum. This is qualitatively understood on the basis that for large values of the electron well widths, the electron wavefunction will cover the whole well where the hole will experience exponential decay, and thus the overlap decreases for large values of $d1$. Furthermore the increase of the widths of the high barriers confining the hole, the energy of the hole will increase a little bit. This very subtle change can however have a big impact
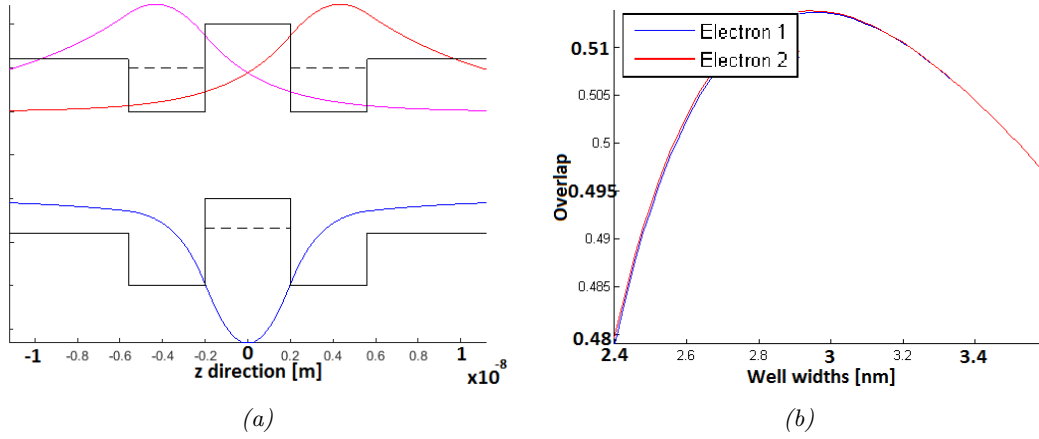
Figure 3.1: (a) Wavefunction landscape in z. Note that the conduction and valenceband are not to scale, however the bands superlattice and energy marks in the wells are. Plotted for $g = 0.6$, $d2 = 4.0$nm, $d1 = d3 = 3.6$ *(b)* The overlaps of both electrons with the hole. Since the both the electrons should be symmetric around the centrum, where also the hole is symmetric about, the lines should be exactly on top of eachother. The small discrepancies are due to the precision of the numerical calculations needed to obtain the plot.

on the overlaps when the hole energy approaches the escape energy as will later be shown and discussed.

For small values of $d1$ the electrons will not be very confined in their respective wells, but will have large parts of their wavefunction in the superlattice, and thus be further away from the hole. All of these effect are seen on figure 3.2. These effects means that it is an optimizable system where the exact calculations are needed to find the optimum instead of just e.g. making a parameter as large as possible. This motivates the idea of moving on to a more complete description of the system.

(a) Low electron well width. (2nm) *(b)* Intermediate electron well width (3nm) *(c)* Large electron well width (6nm)
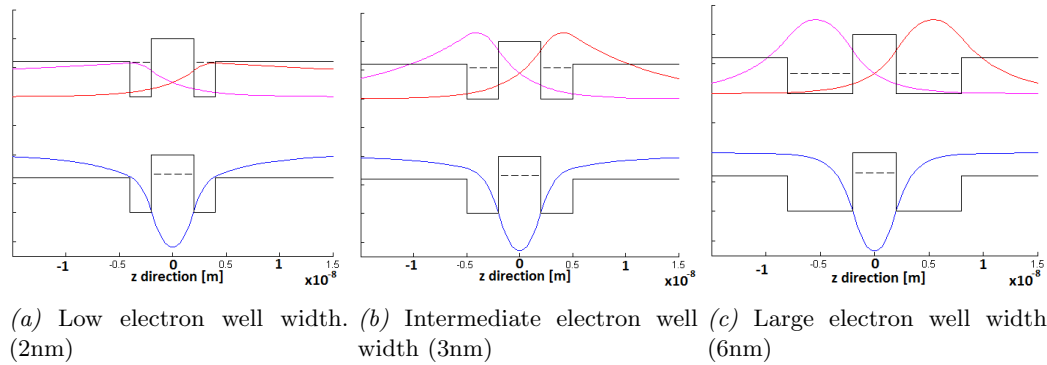
Figure 3.2: The electron and hole wavefunctions as the width of the electron wells increases. The overlaps are smallest in the small and large wells. The largest overlap is found in the intermediate well width picture. Parameters: $g = 0.6$, $d2 = 4$nm

3.1.2   Superlattice parameter

More tendencies will however be checked first. The value of the g parameter is varied and the overlap plot is computed for a couple of values of g. This is seen in figure 3.3. As seen on the figure the overlaps tend to become greater, and the toppoint

seems to move to lower values of $d1$ for increasing g. The physical interpretation
of this is that since the superlattice barrier for the electron rises, it is now possible
to decrease the well width and still have the electron confined, thus making the
overlap with the hole even greater. The curves have been plotted in a fixed interval
in $d1$, however for some parameter values either the hole or the electron will be
unbounded, for these cases the graphs have been cut off. As seen on figure 3.3 the

Figure 3.3: The overlaps as seen in figure 3.1b plotted for different values of g. The reason
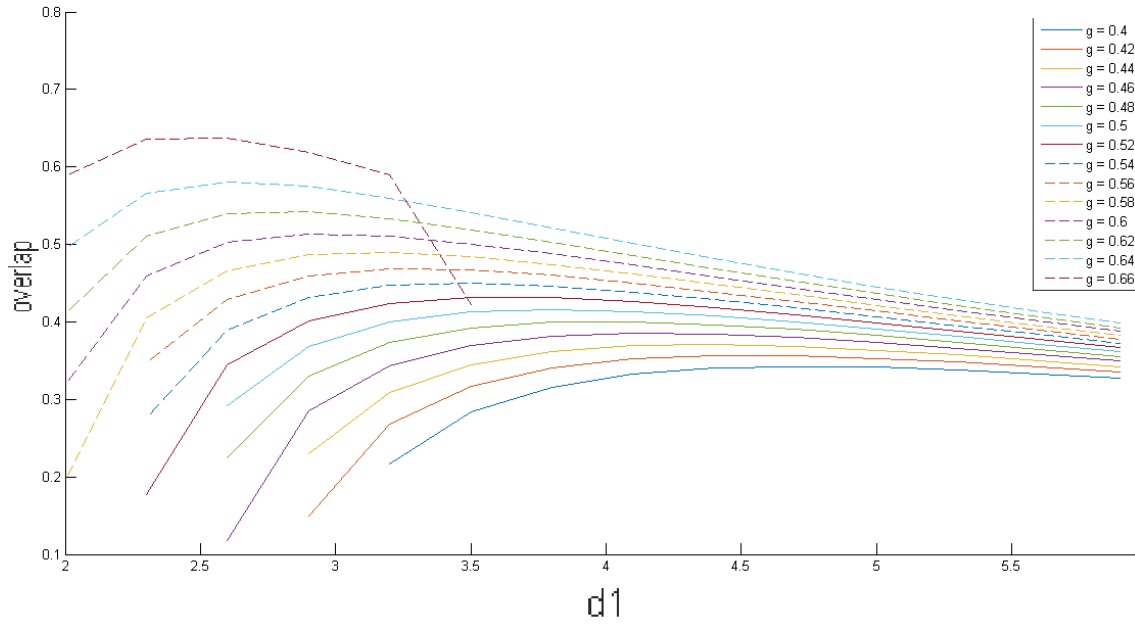for the choice of different intervals is to ensure confinement of both the electron and the hole,
which changes for different values of g.. An anormality is seen for $g = 0.66$ and $d1 = 3.5$nm

graph for $g = 0.66$ looks abnormal. This abnormality is investigated on the basis of
the wavefunctions. A plot like 3.1a is made for $g = 0.66$ and both $d1 = 3.2$nm and
$d1 = 3.5$nm. These two plots are placed on top of eachother in figure 3.4b.

3.1.3   Escaping wavefunctions

As is seen from figure 3.4b the hole wavefunction is much smaller in all the plotted
region. The hole wavefunctions are in both cases normalised. This might suggest
the hole is close to escaping, and therefore will have a larger part of the wavefunc-
tion in the superlattice. The probability of finding the hole in the supperlattice is
calculated from the wavefunctions. For $d1 = 3.2$nm the combined probability of
the hole being in the supperlattice is 14.12%, and for $d1 = 3.5$nm the probability
is 53.65% as also suggested by figure 3.4a. It seems that the hole wavefunction are
very sensitive to small changes in $d1$ in this case.

The reason for $d1$ suddenly becoming a crucial parameter is understood on the
basis of the energies. As is seen in figure 3.4b the hole energy is very close to being
above the superlattice potential - the escape level. The value of the energies are
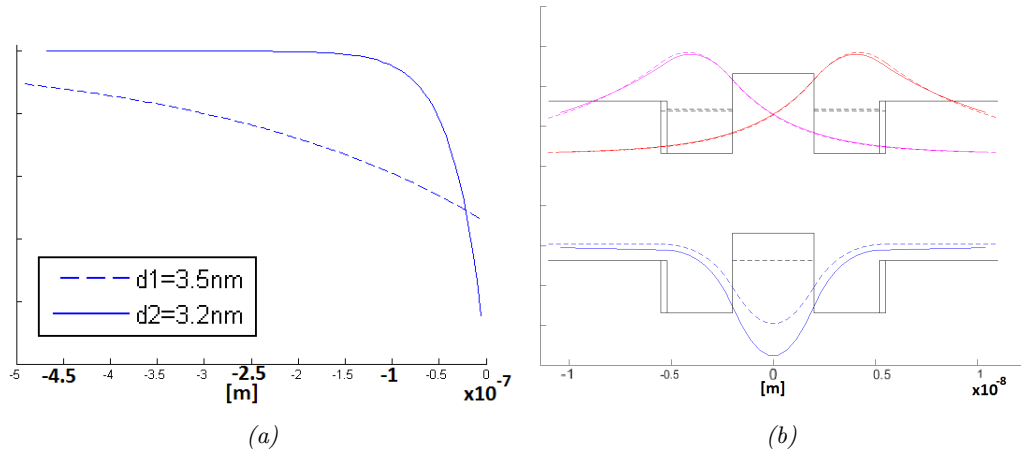$E_h = 3.5259 \cdot 10^{-21}$J at $d1 = 3.2$, $E_h = 3.5400 \cdot 10^{-21}$J at $d1 = 3.5$, where the

Figure 3.4: (a) The part of the wavefunctions for $d = 3.2$nm and $d = 3.5$nm in the leftmost superlattice, plotted in a much larger interval than on figure 3.4b. (b) The wavefunctions for $g = 0.66$ and $d1 = 3.2$nm (Solid lines) and $d1 = 3.5$nm (Dashed lines). Noted is the value of the hole wavefunction seems to be much smaller for $d1 = 3.5$nm in the plotted region. Furthermore the energy of the hole is very close to the escape value of the hole, $v1$.

supperlattice potential is $v1 = 3.5408 \cdot 10^{-21}$J for the hole. Here it is seen that the latter case makes the hole almost escape. To show that it is really the hole energy closing in on the escape energy, the overlap and energy of the hole is plotted as seen in figure 3.5. As mentioned earlier the increase of the barriers for the hole increases the energy a little, but close to the escape level this increase can become very important for the wavefunction and by extension also the overlaps as seen on figure 3.5. The reason why this is not seen on the other lines in figure 3.3 is the resolution of the g and $d1$ parameters.

This escape energy problem indicates that even though the overlap increases for higher values of g, the system becomes much more sensitive to changes in the energy, because the hole might escape.

3.1.4 Hole well width

The last parameter, $d2$, which is the width of the well for the hole is now investigated. Inspired by the previous plots the energy is investigated further. Firstly figure 3.6 shows the overlap for varying values of $d2$ much like figure 3.3 shows it for values of g. The overlaps tend to become smaller and the toppoints tend to move to higher values of $d1$ for increasing $d2$. The interpretation is that when the well for the hole increases, the hole will be much more confined within the well, and thus there is less overlap with the electron in the other regions. The reason for the toppoint moving to higher values of $d1$ can be in order to confine the electron wavefunction more, to decrease its wavefunction in the superlattice.

The energies for both the hole and electron depending on $d2$ has been plotted with the corresponding escape energies in figure 3.7. The energies for the hole decreases as $d2$ increases as expected. The slight energy increase of the hole with increasing $d1$ and $d3$ is understood from considering the extremes. At $d1 = d3 = 0$ the hole inside
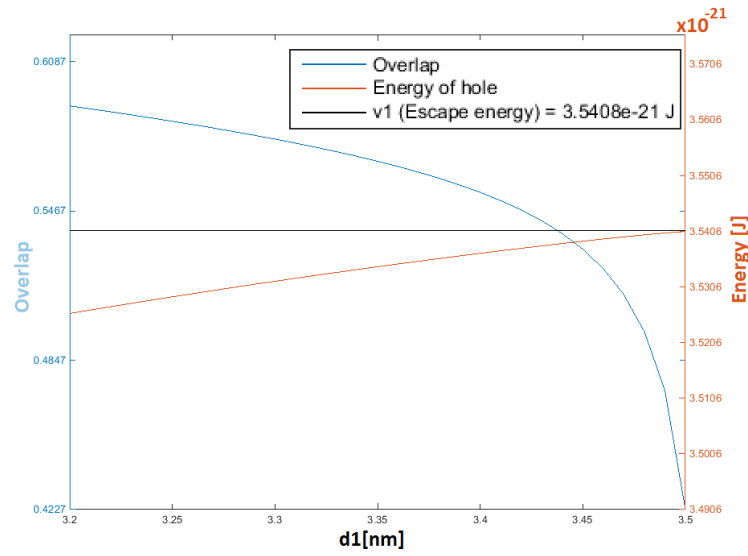
Figure 3.5: The overlap between the hole and electron plotted together with the energy approaching the escape energy (horizontal black line). The overlap seems to react more to energy increases when the energy is close to the escape energy.

the well is bounded only by the superlattice potential which is a smaller potential, and thus the energy of the hole is lower, and vice versa for $d1 = d3 \to \infty$ where it is surrounded by the larger ZB potential. The energies for the electron are completely untouched by the change in $d2$ due to the single well approximation.

Comparing figures 3.6 and 3.7 one finds for the largest overlap that the corresponding energies for both the electrons and the holes are closest to the escape value. So it seems that the biggest overlap is reached when both the electron and hole is closest to escaping and thus spreading their wave function all over the z-axis. This makes sense mathematically because the functions will look more alike when they are far from the double dot system, and thus their overlap is larger. The wavefunctions at one of these high overlaps are plotted in figure 3.8. This is not a physically desirable result however. This result shows that the interpretation of the tendencies is very important, and also that some constraints have to be put on the system - eg. that the particles are localized in the system, and that the lambda level structure needs to be satisfied. The lambda level structure needs to have different values of the energies for the electron in dot 1 and dot 2. Therefore we move on to differing values of the wells.

3.1.5   Differing well widths

The overlaps are expected to roughly stay the same between the hole and the electron in the well that does not change as will be shown later. Small changes are due to the small change in the hole energy, and therefore also the wavefunction as earlier described. The electron in the changing well will change its overlap with the hole following the same tendencies as in the previous section. The overlaps for different values of $d1$ and $d3$ are plotted in figure 3.9 and 3.10. Furthermore choosing to
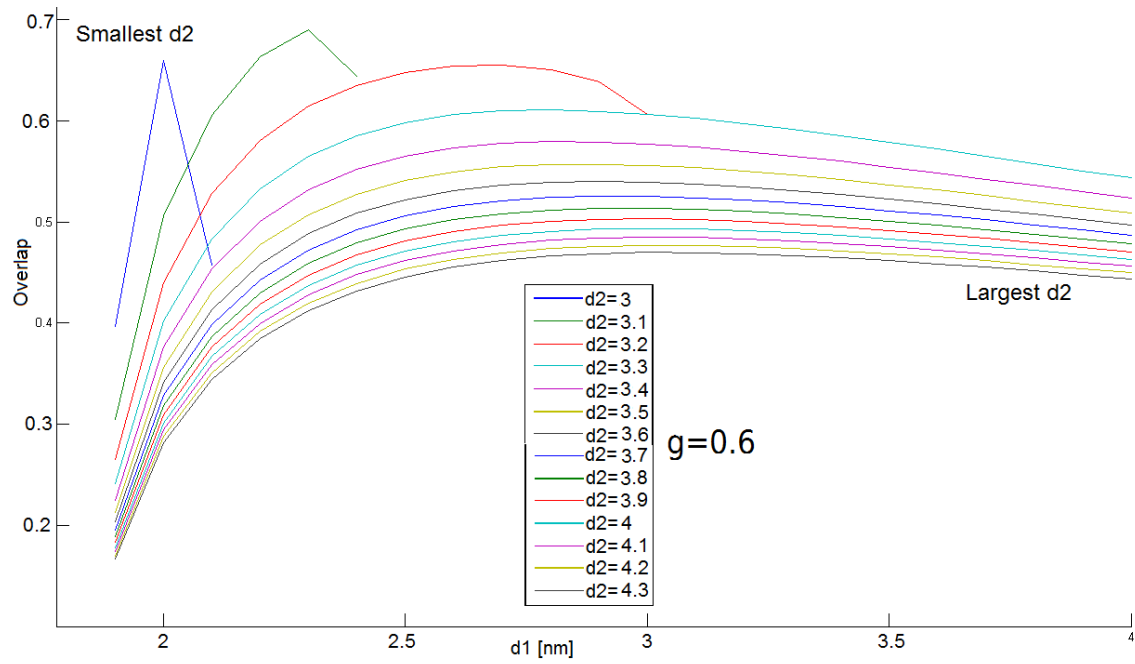
Figure 3.6: The overlap between the hole and electron plotted for different $d2$ values. The overlap is larger for small values of $d2$.
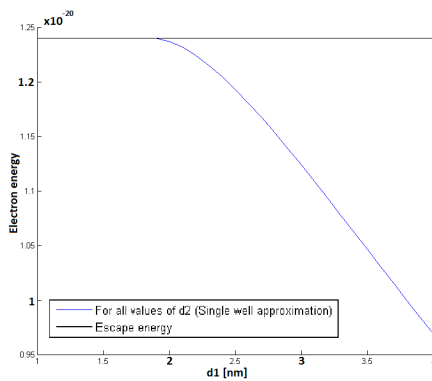
(a) Electron energies. The energy is the same for all values of d2, ignoring the cutoff when the hole energy reaches escape value
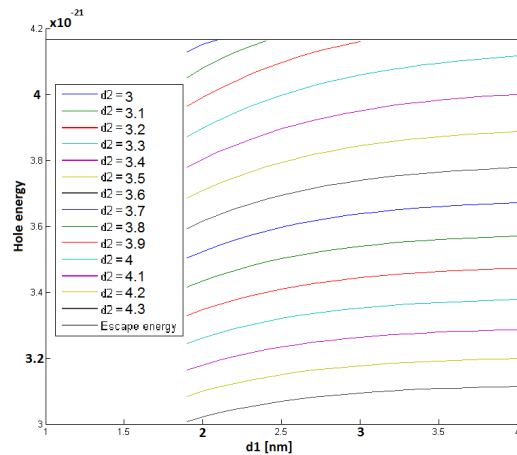
(b) Hole energies.

Figure 3.7: Energy plots for differing $d2$ values for both the holes and electrons. The added horizontal lines correspond to the escape energies for the respective particles.

change one well only alters the overlap significantly for the well in question, the other one is approximately constant. The energies are also plotted in order to see if the system upholds a lambda level structure. These energy plots are seen on figure 3.11 and 3.12. The closer the well widths are the closer the energies are as expected. Of course a specific value of the distances cannot be trusted to find the right lambda level structures and energies, but only the tendencies should be noted.
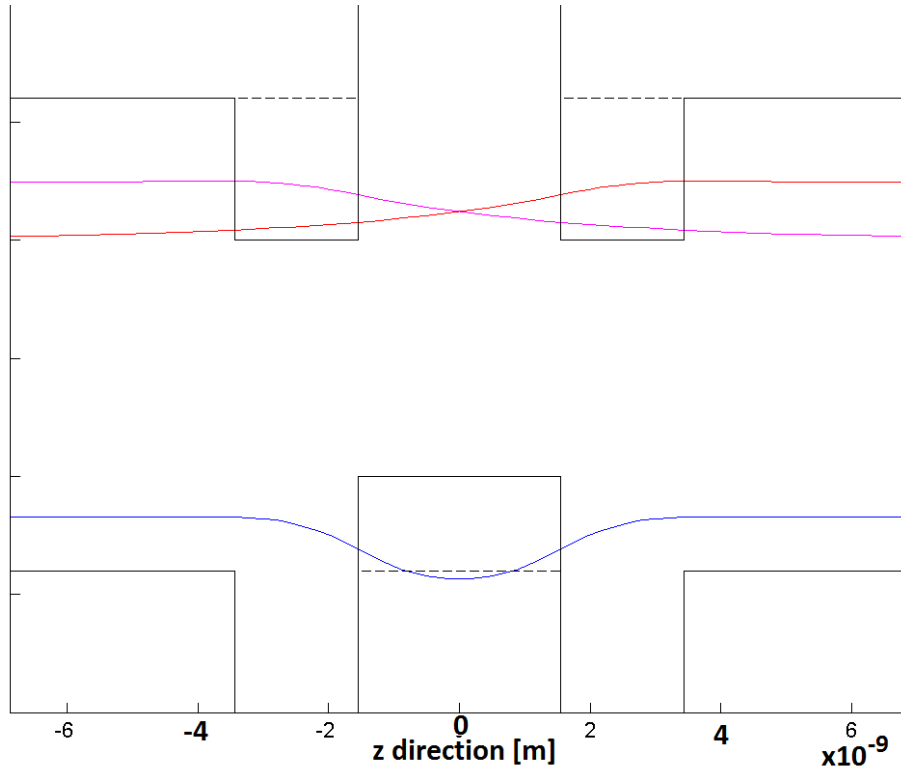
Figure 3.8: The wavefunctions plotted for a large value of the overlap. The wavefunctions are clearly not very confined in the dots. Parameters: $g = 0.6$, $d2 = 3$nm, $d1 = d3 = 2$nm

3.1.6   Summary of the tendencies

The findings of the parameter tendency investigation are as follows. The width of the electron wells have an optimum and should be investigated further. The hole well should in general be small, but at the same time keeping the hole confined. The energy for both the electrons and the holes should be kept well below their respective escape energies in order to ensure confinement. Changing the width of one electron well does not change the overlap significantly for the electron in the other dot, however this might be more an artifact of the single-well approximation and should be investigated. These tendencies can be qualitatively used by an experimenter to adjust the system.

(a) $d3 = 2.2nm$

(b) $d3 = 3.5nm$
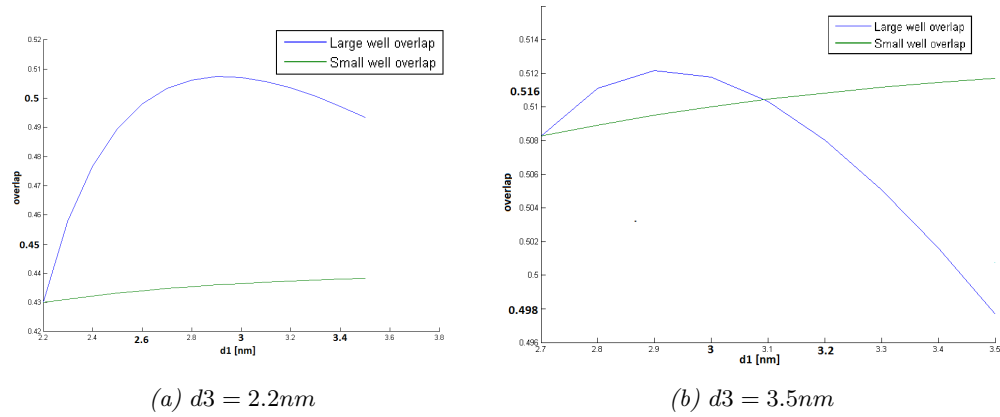
Figure 3.9: For fixed values of $d3$, the width of the small well, the large well is increased and the overlaps are plotted in green (Small well) and blue (Large well). Keep in mind that the reason for the changing absicca interval is in order to keep the small dot the smallest.

(a) $d1 = 2.3nm$

(b) $d1 = 3.5nm$
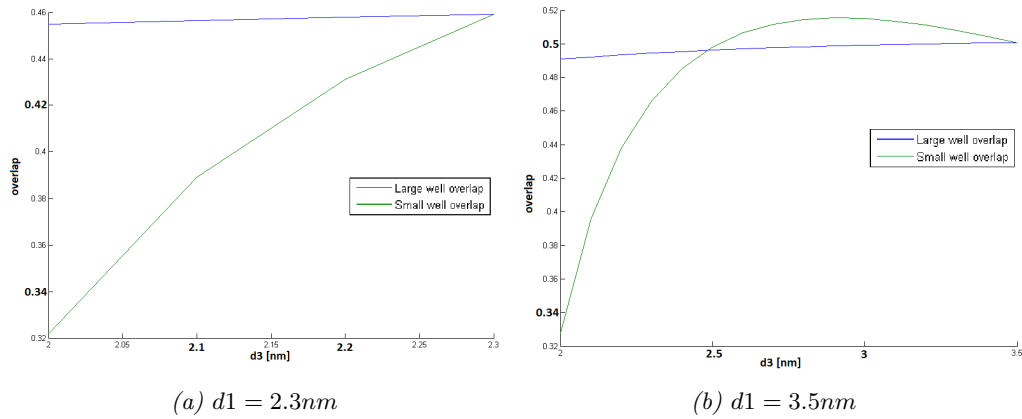
Figure 3.10: For fixed values of $d1$, the width of the large well, the small well is increased and the overlaps are plotted in green (Small well) and blue (Large well). Keep in mind that the reason for the changing absicca interval is in order to keep the small dot the smallest.

(a) d3 = 2.2nm

(b) d3 = 3.5nm
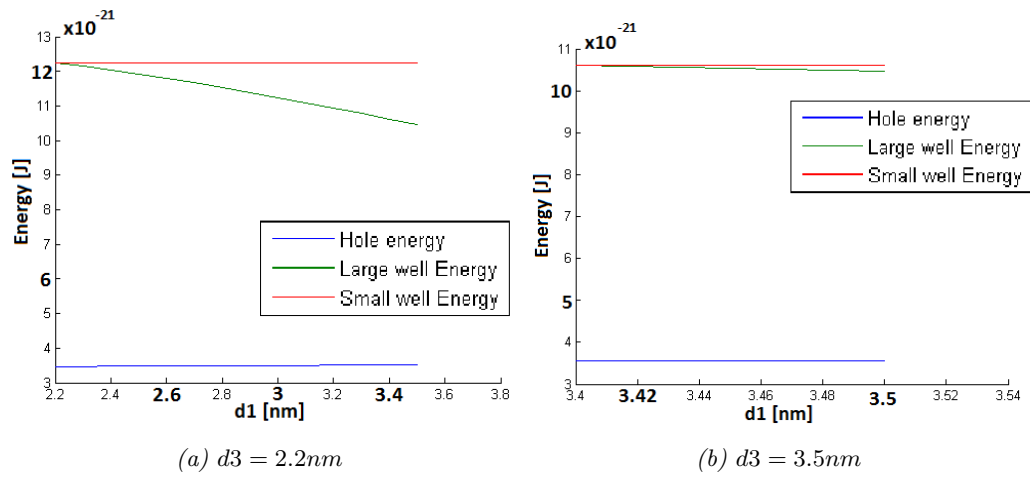
Figure 3.11: For fixed values of the width of the small well, *d3*, the large well is increased and the energies are plotted in red (small hole), green (Large well), and blue (Hole). Keep in mind that the reason for the changing absicca interval is in order to keep the small dot the smallest.
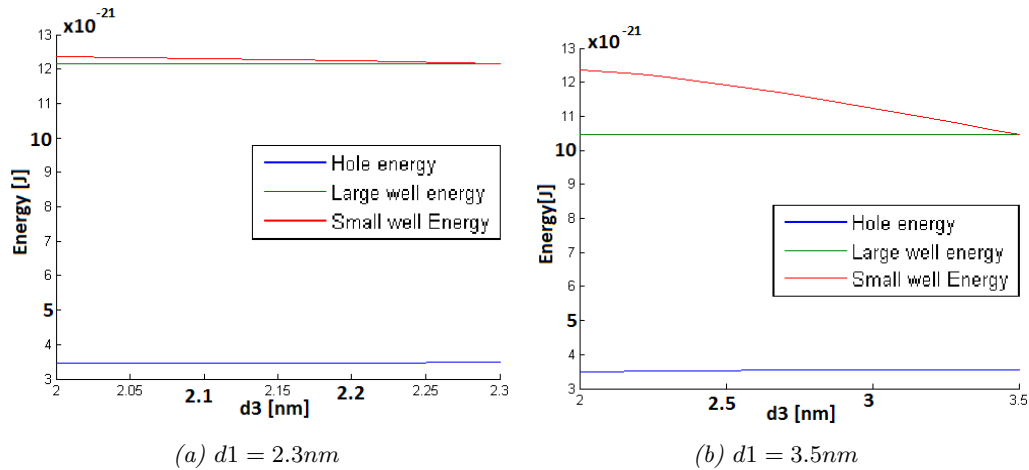
Figure 3.12: For fixed values of the width of the large well, $d1$, the small well is increased and the overlaps are plotted in red (small hole), green (Large well), and blue (Hole). Keep in mind that the reason for the changing absicca interval is in order to keep the small dot the smallest.

3.2 Full potential landscape

Now the wavefunctions are calculated using the full potential landscape for both the electrons and the holes. Since the approximations made already renders the results quantitatively unreliable, the full potential landscape is used to check that the tendencies of the previous section are still consistent, and to get an idea of the confinement of the binding and antibinding wavefunctions. As mentioned in section 2.1.3 the dot sizes should be different, this is also confirmed by doing the full potential landscape calculations and seeing the overlap between the antibinding state with the hole is zero when the dots are the same width. This is due to the odd parity of the antibinding wavefunction and the even parity of the hole wavefunction cancelling out.

How the overlap and energy change, is especially important since we still wish to optimize the overlap while still having the electron binding and anti binding states confined in each well. By calculating different parameter shifts it is possible to see if it follows some of the same tendencies as with the single well approximation.

3.2.1 Overlap while varying d1 and d3

First we look at the overlap while varying $d1$, $d3$ and keeping $d2$ at a constant value. This is done to see if the tendencies are similar to the single well approximation. The binding wave functions in figure 3.13a shows pretty much the same tendency as for the single well approximation, which is that the highest overlap is achieved when the two electron wells have equal width. Even though this might be the highest overlap, the confinement in a specific is in this case not very good as shown in figure 2.1.

The anti bonding achieve some lower values in the overlap as seen in figure 3.13b, and reaches an overlap of zero, when the electron wells have equal width. This can also be seen from the symmetry of the anti binding- and hole wave function.
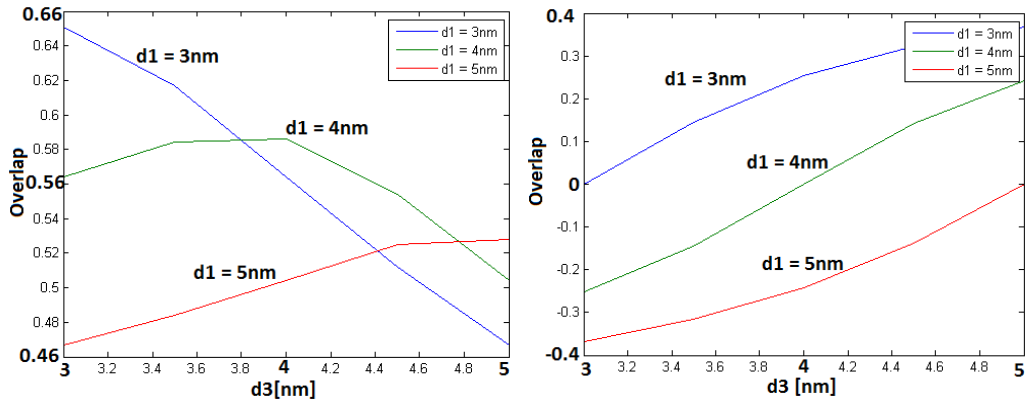
(a) Binding wave function overlap, as a function of $d3$, with constant $d2 = 5$nm and varying $d1$

(b) Anti binding wave function overlap, as a function of $d3$, with constant $d2 = 5$nm and varying $d1$

Figure 3.13: Binding and anti binding wave function overlap with the hole wave function

3.2.2 Energy while varying d1 and d3

We also want to investigate the energy in the system, since this can have an influence on the overlap as well, due to the electron and hole being close to escaping their respective wells.
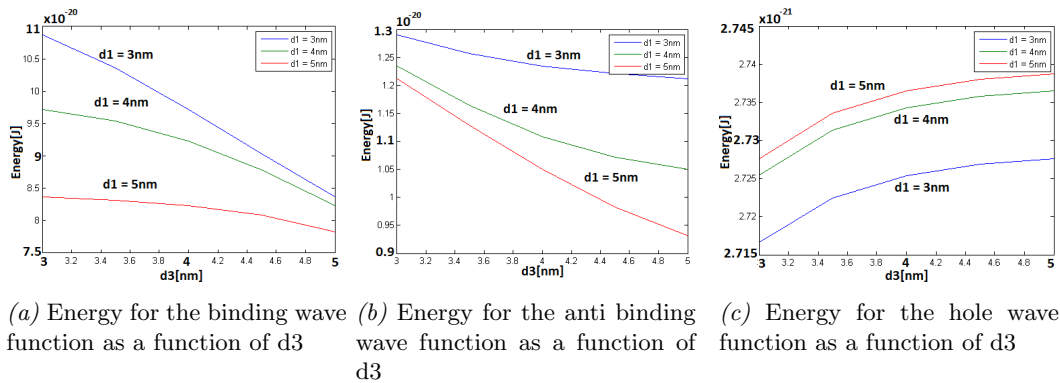
(a) Energy for the binding wave function as a function of d3

(b) Energy for the anti binding wave function as a function of d3

(c) Energy for the hole wave function as a function of d3

Figure 3.14: Energys for the binding- anti binding- and hole wave functions

Here we see the same tendencies as we did for the single well approximation. The binding wave function energy drops more rapidly than the anti binding due to the binding being confined in the dot with width d3. Simultaneously one of the barriers for the hole gets wider, and hereby making energy of the hole rise. The hole also has the largest energy when d1 is larger due to having a bigger barrier on each side of the dot.

3.2.3 Increasing d2 for different well sizes

The effect of the hole well is investigated. A plot is made for increasing $d2$ for different values of $d1$. As a first note when calculating the plots for this, the antibinding wavefunction is too energetic to be confined in the dots for small values of $d2$. The energy tendency as a function of $d2$, much like figure 2.2 for equal electron

well sizes, is plotted for inequal well widths in figure 3.15. The energies approach eachother but they have an extra asymptote separation. This is because for $d2 \to \infty$ the energy separation is the energy difference between the two dots of inequal size. This separation ensures the lambda level structure is obeyed. The calculations also
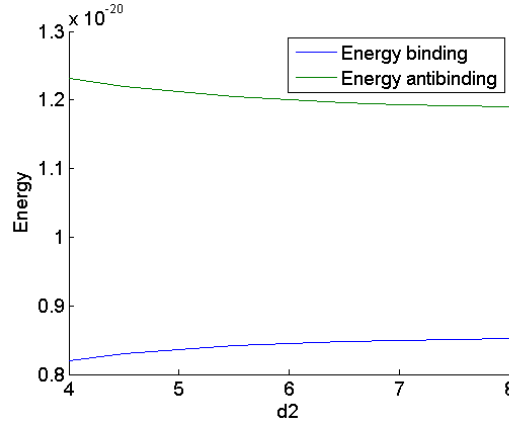
Figure 3.15: The overlap for the binding and antibinding wavefunction as $d2$ increases for different well sizes. $d1 = 3$ and $d3 = 5$

show that increasing $d1$ makes the hole not confined for low values of $d2$, which is understood with the same arguments about increase of hole energy in the treatment of the single well approximation. But mostly the overlap decreases as the hole well width, $d2$ increases, expected by figure 3.6. This is plotted in figure 3.16. The initial rise in overlap on figure 3.16 *(b)* is due to the hole not being confined as discussed.

(a) $d1 = 2nm$ *(b)* $d1 = 3nm$
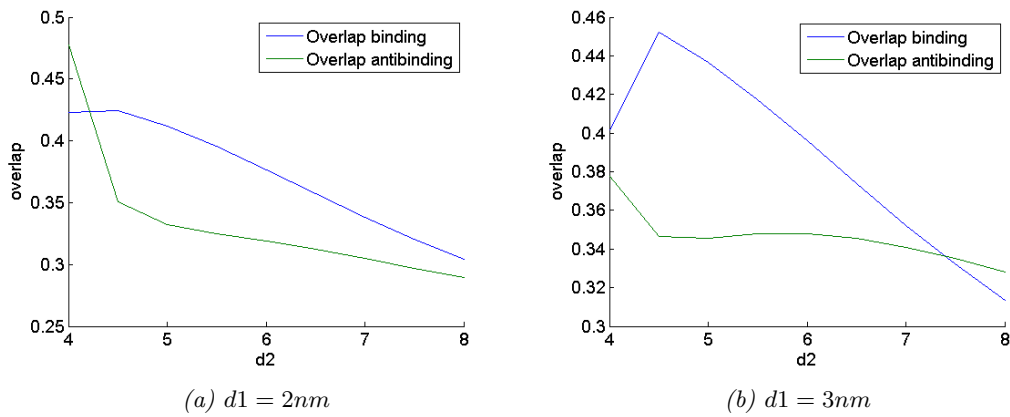
Figure 3.16: The overlap of the binding and antibinding electron wavefunction with the hole for increasing d2. Plotted on figures with different $d1$. Parameters: $g = 0.66$ $d3 = 5$nm

On figure 3.17 wavefunctions are plotted for different values of d2.The lack of hole confinement in 3.17*(a)* is apparant from the wavefunctions.

3.2.4   Confinement in each well

Finally the confinement in the wells are checked. The confinement in well 1 for two different values of the well size are plotted on figures 3.18 and 3.19. The binding
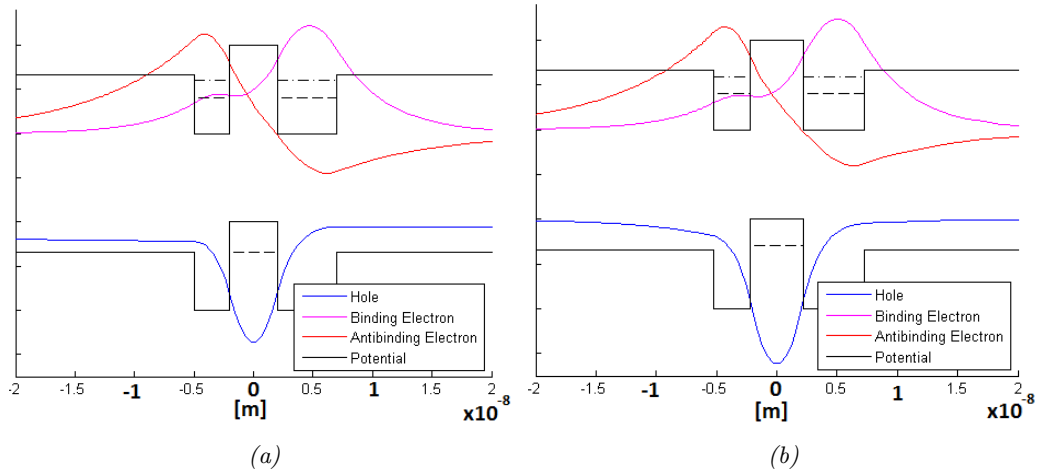
Figure 3.17: Electrons and hole wavefunction in the potential landscape for two specific values of $d2$. Note how the hole wavefunction does not go to zero (defined from the top of the hole well in the figure) towards the left in *(a)* within the plotted region. Parameters: $d3 = 5$nm, $d1 = 3nm$, $g = 0.66$.

wavefunctions are primarily situated in dot 2 and the antibinding in dot 1. The figures show that for increasing the separation distance, $d2$, the probability for finding the particle in the right dot is increased, as well as the probability in the wrong dot is decreased. Furthermore changing the small value of dot 1 from 2 nm to 3nm increases the antibinding confinement. This is due to the well being too small. All in all the binding wavefunction is more localised than the antibinding, due to the antibinding having higher energy and thus being closer to escaping.
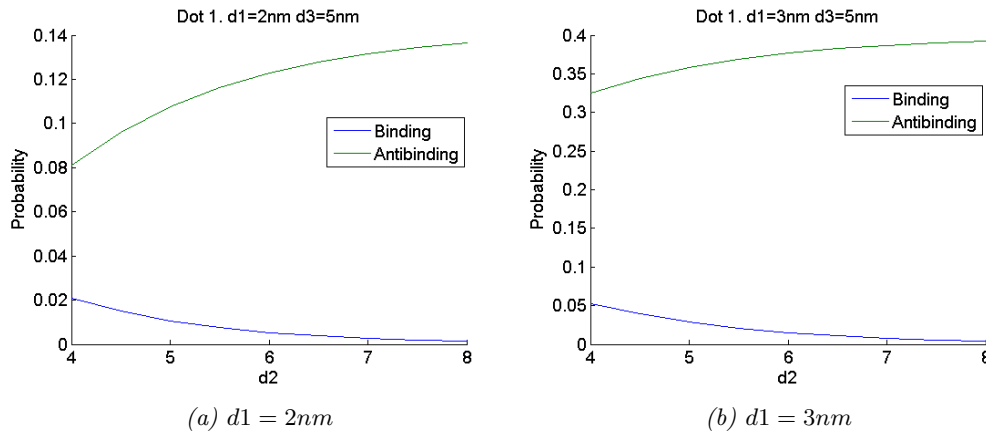
Figure 3.18: The norm square of the wavefunction within dot 2 (where the antibinding should be located). The localisation goes up from *(a)* to *(b)* for the antibinding dot, because the dot width increases. Parameters: $g = 0.66$, $d3 = 5$nm.

3.2.5   Summary

This section has shown the tendencies of the single well approximation are also valid for the full potential landscape. The difference between the two electron well widths should be of notable size to keep the overlap between antibinding and hole nonzero.
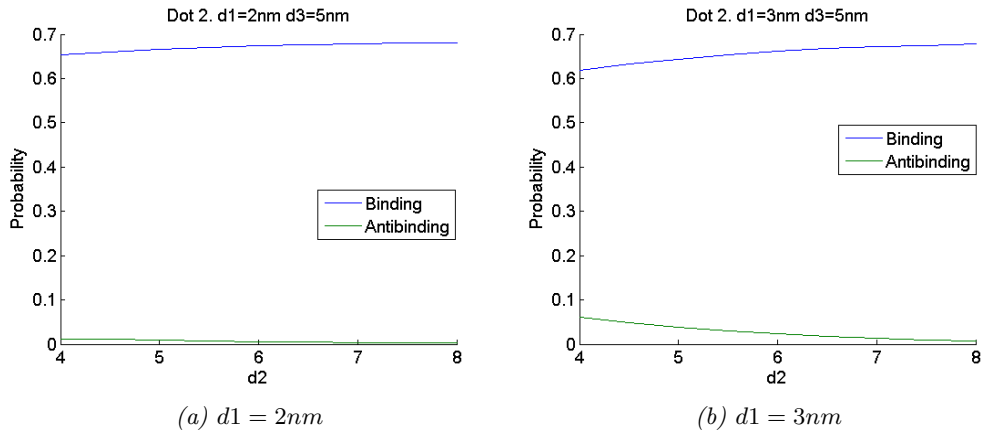
Figure 3.19: The norm square of the wavefunction within dot 1 (where the binding should be located). The localisation goes up from *(a)* to *(b)* for the antibinding dot, because the dot width increases. Parameters: $g = 0.66$, $d3 = 5$nm.

The lambda level structure needs to be uphold, but that is taken care of by having a larger electron well width difference. The well width difference still needs to be no bigger than having the energy of the antibinding be far enough from escape energy level to keep it confined, or that one of the dots is too large to have a notable overlap. For the electron wavefunctions to be confined in their respective well the separation distance should be large, but this reduces the overlap so an optimum has to be found.

Chapter 4

Improving approximations

4.1 The Exciton

The excited state, $|3\rangle$ in figure 1.2, is a charged exciton. An exciton can be created, if a semiconductor system receives some energy that exceeds the gap energy in the semiconductor material. This usually comes in the form of photons, which enables an electron in the valence band to get excited and able to sit in the conduction band. This leaves a hole in the valence band, and the electron and hole feels an attractive force between them, called the coulomb force. The exciton is the electron-hole pair that comes from the excitation, when the electron and hole is in a confined bound state. The electron orbits the hole, and is seen as a new particle, the exciton. Adding the initial electron in the system one obtains a negatively charged exciton.
A negatively charged exciton wave function consists of both the electrons and hole wave functions, which all changes due to the coulomb interaction between the three particles. The charged exciton wave function is important since it gives an understanding of how the system actually behaves.

4.1.1 Computing the exciton wave function

As a simple initial calculation a regular exciton will be calculated as in [16]. The computation of the exciton wave function requires the use of the post Hartree-Fock method, configuration interaction. Here the Hamiltonian gets corrected by the contribution from the coulomb interaction which makes it rather more complicated to solve. How to compute the exciton wave functions is explained in greater detail later on. The coulomb interaction will also be discussed in greater detail.

4.1.2 The Coulomb interaction

In classical electrostatics dealing with point charges the coulomb interaction is known as: $V_C = \dfrac{1}{4\pi\epsilon} \dfrac{e^2}{|\boldsymbol{r} - \boldsymbol{r}'|}$ for the resulting potential energy stored in a system of two point charges with the separation $|\boldsymbol{r} - \boldsymbol{r}'|$ between them. In the quantum mechanical description the coulomb interaction between two particles with known probability distributions is given as:

$$V_C = \frac{q^2}{4\pi\epsilon} \int \int \frac{|\phi_1\left(\boldsymbol{r_1}\right)|^2 \, |\phi_2\left(\boldsymbol{r_2}\right)|^2}{|\boldsymbol{r} - \boldsymbol{r}'|} \, \mathrm{d}\boldsymbol{r_1} \mathrm{d}\boldsymbol{r_2} \tag{4.1}$$

An operator for this two particle interaction in second quantization can be found using the general approach described in section 17.4 of [7] equations 17.26, 17.41, 17.42.

$$\hat{\psi}^{\dagger}(x) = \sum_{\alpha} \left(\phi_{\alpha}(x)\right)^{*} C_{\alpha}^{\dagger}, \quad \hat{\psi}(x) = \sum_{\alpha} \phi_{\alpha}(x) C_{\alpha} \tag{17.26}$$

$$([7])$$

An additive pair operator can be expressed in second quantization as:

$$\hat{H}_C = \frac{1}{2} \sum_{\alpha\beta\gamma\delta} v_{\alpha\beta,\gamma\delta} C_{\alpha}^{\dagger} C_{\beta}^{\dagger} C_{\delta} C_{\gamma} \tag{17.41}$$

$$([7])$$

Where,

$$v_{\alpha\beta,\gamma\delta} = \int \int \phi_{\alpha}^{*}(\boldsymbol{r}) \phi_{\beta}^{*}(\boldsymbol{r'}) v(\boldsymbol{r},\boldsymbol{r'}) \phi_{\gamma}(\boldsymbol{r}) \phi_{\delta}(\boldsymbol{r'}) \, \mathrm{d}\boldsymbol{r}\mathrm{d}\boldsymbol{r'} \tag{17.42}$$

$$([7])$$

and v is the interaction strength, i.e. $\dfrac{q^2}{4\pi\epsilon}\dfrac{1}{|\boldsymbol{r}-\boldsymbol{r'}|}$. r and r' describing particle one and 2 respectively.

Thus we see, combining corresponding creation/annihilation operators with their respective wavefunctions to obtain factors of the form of (17.26) [7]. This leaves us with the field operators such that the operator is on the form:

$$\hat{\boldsymbol{H}}_{\boldsymbol{C}} = \frac{1}{2} \sum_{nm} \int \int \frac{q^2}{4\pi\epsilon} \frac{\hat{\psi}_n^{\dagger}(\boldsymbol{r}) \hat{\psi}_m^{\dagger}(\boldsymbol{r'}) \hat{\psi}_m(\boldsymbol{r}) \hat{\psi}_n(\boldsymbol{r'})}{|\boldsymbol{r}-\boldsymbol{r'}|} \, \mathrm{d}\boldsymbol{r}\mathrm{d}\boldsymbol{r'} \tag{4.2}$$

This addition to the hamiltonian is too large to be considered as a small perturbation. This means that not only will considering the coulomb interaction change the energies, it will also change the wavefunctions. This means that more intricate variational methods need to be applied to obtain solutions for the full description of the system.

Inspired by the works of [16] the method chosen is configuration interaction. A post Hartree-Fock method that in principle will yield correct results for a full configuration interaction and not just approximations to the solution, however this requires very large computation times since one includes all the space spanned by the single particle basis. In [16] a neutral exciton (one electron and one hole) is calculated, and we shall as to begin with try to follow the calculations to see if the charged exciton wavefunction is desired to pursue. [16] states in their paper that for including the 12 lowest single particle states in their calculations yield accurate convergence for the lowest few single particle states.

4.1.3 Configuration interaction method

Configuration interaction describes the corrected wave functions by making the new eigenvectors consist of linear combinations of Slater determinants[20]. Instead of the

one-particle time-independent perturbation theory for small perturbations, which gives the energy correction $\langle n| H^{(1)} |n\rangle = E^{(1)}$, we have a multi-electron system with coulomb interaction between the particles. This gives us the full Hamiltonian described as

$$H = H_0 + H_c \tag{4.3}$$

Where H_0 is the standard Hamiltonian in three dimensions

$$H_0 = -\frac{\hbar}{2m_e}\nabla^2 + V \tag{4.4}$$

and H_c is the Hamiltonian which comes from the coulomb interaction between the charged particles in the system, that is the electrons and holes. As we have already derived, the operator H_c is given by

$$H_c = \frac{1}{2}\sum_{nm}\iint d\mathbf{r}d\mathbf{r'}\frac{\boldsymbol{\psi}_m^\dagger(\mathbf{r})\boldsymbol{\psi}_n^\dagger(\mathbf{r'})\boldsymbol{\psi}_n(\mathbf{r'})\boldsymbol{\psi}_m(\mathbf{r})}{\kappa|\mathbf{r}-\mathbf{r'}|} \tag{4.5}$$

Where $\kappa = \frac{q^2}{4\pi\epsilon}$ and the field operators $\hat{\boldsymbol{\psi}}_{m/n}(\mathbf{r})$ is for the electron and hole respectively. The Hamiltonian H_c can also be written in its matrix form, and H_c then becomes

$$H_c = \begin{bmatrix} \langle n_1| H_c |n_1\rangle & \langle n_2| H_c |n_1\rangle & \cdots & \langle n_n| H_c |n_1\rangle \\ \langle n_1| H_c |n_2\rangle & \langle n_2| H_c |n_2\rangle & \cdots & \langle n_n| H_c |n_2\rangle \\ \vdots & \vdots & \ddots & \vdots \\ \langle n_1| H_c |n_n\rangle & \langle n_2| H_c |n_n\rangle & \cdots & \langle n_n| H_c |n_n\rangle \end{bmatrix} \tag{4.6}$$

To find the eigenfunctions the Hamiltonian H has to be diagonalized, which means that the new system is written in its own eigenvector basis. The matrix that has to be diagonalized is

$$H = H_0 + H_c = \begin{bmatrix} E_1 \langle n_1| H_c |n_1\rangle & \langle n_2| H_c |n_1\rangle & \cdots & \langle n_n| H_c |n_1\rangle \\ \langle n_1| H_c |n_2\rangle & E_2 \langle n_2| H_c |n_2\rangle & \cdots & \langle n_n| H_c |n_2\rangle \\ \vdots & \vdots & \ddots & \vdots \\ \langle n_1| H_c |n_n\rangle & \langle n_2| H_c |n_n\rangle & \cdots & E_n \langle n_n| H_c |n_n\rangle \end{bmatrix} \tag{4.7}$$

The Hamiltonian H is after diagonalization in the eigenvector basis, and the energies and wavefunctions of the exciton are found.

The value of a matrix element of H_c on matrix form needs to be calculated. In order to do this, the action of the coulomb hamiltonian on a state needs to be calculated. Considering initially a state vector described with field operators[1]

$$|\phi(r)\rangle = \int d\boldsymbol{r}\phi(r)\psi^\dagger(r) |\text{vac}\rangle = \int d\boldsymbol{r}\phi(r) |r\rangle \tag{4.8}$$

Such that the wavefunction can be retrieved the usual way. $\langle r'|\phi(r)\rangle = \int d\boldsymbol{r}\phi(r) \langle r'|r\rangle = \phi(r')$. An annihilation field operator acting on a state vector will then correspond

---

[1]Formally the vacuum state in a solid state material should be the Fermi sea instead, however treating the particles as just being in an external potential, disregarding the solid state material (envelope approximation) we avoid getting into further considerations such as particle/hole transformations of the creating and annihilation operators.

to:

$$\psi(r) \left| \phi(r) \right\rangle = \int dr' \phi(r') \psi(r) \psi^\dagger(r') \left| \text{vac} \right\rangle \tag{4.9}$$

This can be rewritten using the commutation relations for the field operators (eq. (17.21) [7]).

$$= \int dr' \phi(r') \left(\delta(r - r') - \psi^\dagger(r) \psi(r) \right) \left| \text{vac} \right\rangle \tag{4.10}$$

$$= \phi(r) \left| \text{vac} \right\rangle \tag{4.11}$$

And as such a matrix element can be evaluated (The factor of 1/2 dissapears due to 2 spins pr. orbital):

$$\langle ij | \hat{H}_C | i'j' \rangle = \frac{q^2}{4\pi\epsilon} \iint \frac{\phi_i^*(r) \phi_j^*(r') \phi_j(r') \phi_i(r)}{|r - r'|} dr dr' \langle \text{vac} | \text{vac} \rangle \tag{4.12}$$

Where the inner product over the vacuum state is 1. These matrix elements are problematic to evaluate due to the divergence in $r = r'$. However using Cauchy's residue theorem to integrate around the divergences in the complex plane allows the integral to be calculated.

4.1.4   Cauchy's Residue theorem

Cauchy's residue theorem is a powerful tool, used when evaluating complex analytical functions in a given area. Typically it is used to evaluate integrals in which the integrated function diverges, usually because the function is not defined at some points in the integral, referred to as poles (dividing by zero, being the most common type of pole). A function can have several poles in a given area, which all need to be evaluated using the Residue theorem. The Residue theorem is given by:

$$\oint_C f(z) dz = 2\pi i \sum_{k=1}^{n} Res\left(f(z), z_k \right) \tag{4.13}$$

Where $f(z)$ is the function which is being evaluated with poles at points z_k. The full formulation of the theorem can be found in appendix A.2.

With cauchy's residue theorem in place, we have a method of avoiding the divergences when trying to solve the coulomb interaction matrix elements. The method is described in appendix A.5, and the final result is that the matrix elements are:

$$\langle ij | \hat{H}_C | i'j' \rangle = -\frac{e^2 \pi}{\epsilon} \iiint dq\, dz\, dz' \exp\left(-q \left| z - z' \right| \right) Z_i(z) Z_j(z') Z_{i'}(z) Z_{j'}(z') \tag{4.14}$$

$$\times \int dr\, r R_i(r) R_{i'}(r) J_0(qr) \int dr'\, r' R_j(r') R_{j'}(r') J_0(qr') \tag{4.15}$$

$\hat{H}$ will have to be calculated for only a limited number of configurations to save computation time. However the first couple of exciton wavefunctions will have to have converged.

The change of the first element in $\hat{H}$ will get smaller the more wave functions that

are added, and when about 12 wave functions is taken into consideration the change of the ground state exciton will be so small that it can be neglected, meaning that the final energy for the ground state exciton is approximated very close to the actual value [16].

To be able compute all these energies, the system has to be simulated on a computer. Configuration interaction method is very CPU heavy, and is therefore limited to systems that consists of relatively few particles. To be able to simulate with the configuration interaction method, it its important to only consider a small system or have a powerful computer at your disposal.

4.1.5   The numerical solution to the exciton wavefunction

The implementation of the mathematics descriped in the previous section is implimented via a script (MatLab). The script seeks out to find the matrix elements in the coulomb interaction hamiltonian in the configuration interaction calculations. These calculations are based on the ones in [16]. The script calculates the constants used in the piecewise description of the electron and the hole wavefunctions along with the energies for given quantum numbers. It also sorts the energies from lowest to highest. The numerical coulomb integral is solved by a riemann sum, $\sum f(z)\Delta_Z$, which needs a step size and a cutoff value, which is chosen such that the riemann sums have converged, i.e. do not change the value within a set tolerance when the step size is decreased or the cutoff is increased - details about ensuring uniform convergence of these sums are found in appendix A.3.

After this the script runs 4 nested loops over the combinations of electrons and hole matrix elements. Each matrix element starts with choosing the correct wavefunction and energy, and then moves on to calculating the corresponding integrals. The crucial parts of the code are (in the loop at least) vectorized as much as we were able to do. The parts that are not completely optimized are not part of any loops and scale as N^0 (N being the steps in the riemann sum), which implies that since the computation time is a few seconds in the beginning of each run of the script, it is not really prioritizable to optimize them.

In spite of the steps taken to optimize the code it is still painfully slow. Each matrix element of the hamiltonian takes more than an hour to calculate on a computer. Trying to reach the results of [16] with the 12 lowest single particle states for both the electron and hole leads to a matrix of 144^2 elements, which will be more than a year to calculate. Even taking into account that the matrix is symmetric and thus reducing the computation by about a half, it is still a long time. Reducing the computation to only take the 4 lowest single particle energies will take around a week. This will in principle lead to a matrix which can calculate the wavefunctions for an exciton. The excited state in the real lambda level structure, figure 1.2, is not an exciton but a negatively charged exciton. This adds further computation time to the problem and makes it almost impossible to calculate on regular laptop computers. Using the charged exciton wave function for dipole moment optimization requires new calculations for each parameter increment, making it horribly absurd to pursue. Matlabs profiler has been used to identify the computationally heavy

elements of the script, and the problems are seen in figure 4.1. It is clear that the shear amount of times the summing over a matrix occurs is the thing that takes the most time in the script. The use of the real charged exciton as a wavefunction

```
2064.51 2004975  216          [zfun,zmfun]=meshgrid(elez.*e
6582.54 2004975  217          runsumzm=runsumzm+sum(...
         218              sum(...
         219                  zfun.*zmfun.*...
         220                  exp(-q.*abs(zcell-zmcell)
  25.85 2004975  221         end
   4.72  400995  222       end
         223       %The complete overlap for a the given
34432.01   80199  224     runsum=runsum+...
         225       integral(@(s)(s.^(1+ni+nim).*exp(-s.^2).*m
         226       mfun('L',kim,nim,s.^2).*besselj(0,q*s*bsca
         227       * ...
         228       integral(@(s)(s.^(1+nj+njm).*exp(-s.^2).*m
         229       mfun('L',kjm,njm,s.^2).*besselj(0,q*s* bsc
         230       * ...
         231       runsumzm;
   0.33   80198  232 end
            8  233 toc
         234 %The coulomb matrix hamiltonian.
< 0.01      8  235 Hc((i-1)*4+j,(im-1)*4+jm)=runsum*deltaq*9.1102
            8  236             end
< 0.01      8  237           end
< 0.01      2  238         end
         239     end
         240   ond
```
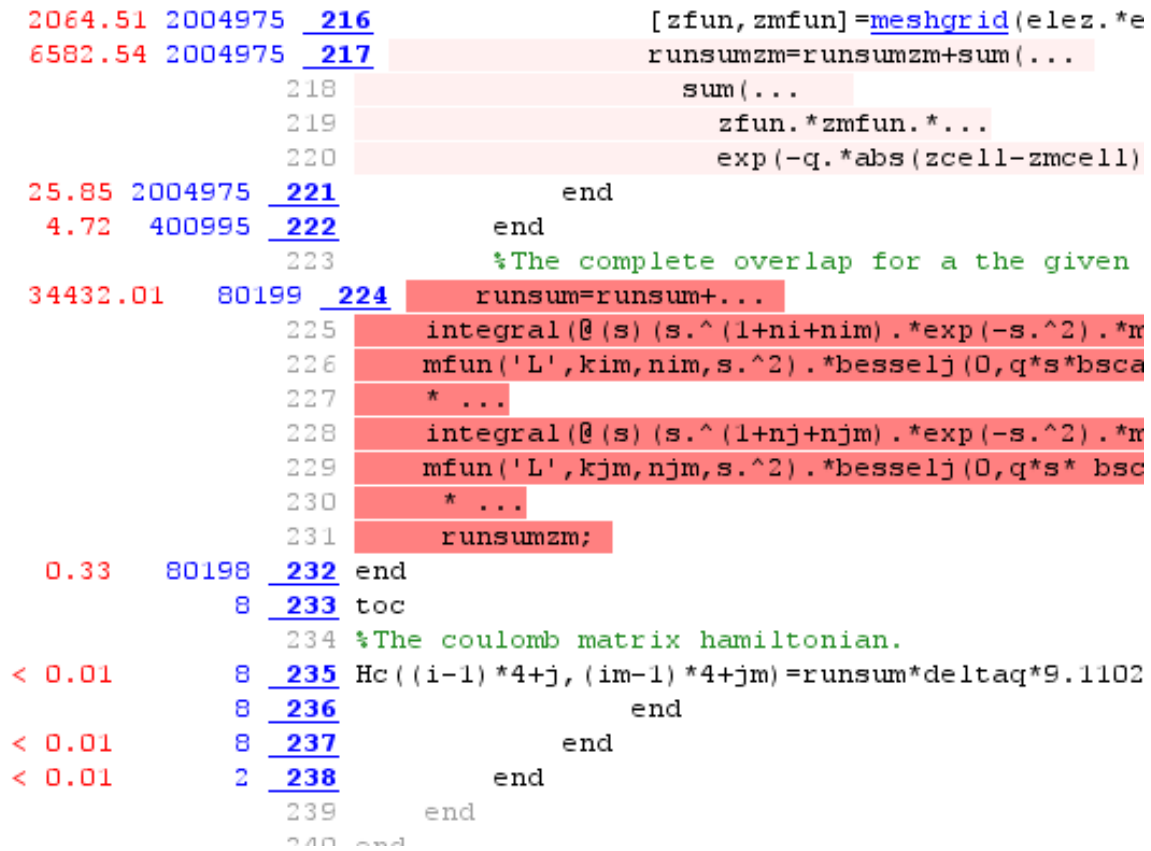
Figure 4.1: The Matlab profiler showing the computationally demanding part of the script. As seen it is the summing over the functions.

is with our remedies too time consuming, and thus we shall seek to approximate it in the single particle picture. The calculations followed here can however form the basis for any future treatment of this problem.

Chapter 5

Outlook and conclusion

5.1 Outlook

Due to time restrictions and the fact that the computation of exciton wave functions via the configuration interaction method is very time consuming, a decision was made to look at the overlap between electron and hole wave functions instead to compute approximated results. Here it would be ideal to to get the actual charged exciton wave functions out, by either writing a new and more optimized script in MATLAB or take the code which we wrote and optimize it further and make it run on multiple cores to make it run faster on a supercomputer cluster. Even with a supercomputer one would have to calculate the charged exciton wavefunction several times since the wavefunction would change for each new increment of a parameter. Therefore we would not have been able to get results out which we did with the single particle approximation within the course of the project.

The system has a potential that makes the hole not being confined in the well in the single particle picture. Instead a super lattice was put in, which had the potential gV_0 where g was a constant between 0 and 1 and V_0 the potential of the electron wells. This was done in order to be able to compute the wave functions in the system, so we could optimize the overlap of the electron- and hole wave functions. For more precise results the potential without the superlattice should be implemented in the calculations.

For the energy of the charged exciton, instead of doing a configuration interaction, one could have made a simple energy correction with first order perturbation theory. This would only require a calculation equivalent of one matrix element in the configuration interaction. However the script should be modified to include an extra electron. This was determined to be too time consuming compared to the yield of such a calculation. A further investigation is left for others to pursue.

5.2 Conclusion

During the time period of this project, we have worked on optimizing a quantum double well potential system, to make a quantum gate with as efficient gating as possible. This means the dipole moment, and by extension the overlap between the envelope of the electron wave functions and the charged exciton wave function

should be optimized. This is due to the gating process being a STIRAP-process, which can operate faster without being a non adiabatic process if the dipole moment is as high as possible. Being adiabatic means not populating the exciton level and losing information by radiative decay.

The wavefunctions for the non interacting particles in the system have been calculated. Two different suggestions for the radial wavefunction were proposed, one corresponding to a parabolic confinement potential and another for a flat circular well structure, of which the latter was argued to be more realistic.

The envelope part of the dipole moments in the interband transitions was calculated in order increase the understanding of the full dipole moment, which is to be optimized. The optimization was primarily done by tweaking 4 different parameters, the width of the electron wells, width of the hole well and the super lattice, i.e. the g parameter.

When the dots were of equal size, it was possible to force the electron to be confined in one of the dots, by making it a superposition of the binding and anti binding states. But due to tunnelling effects and a short transition time it would oscillate between the two electron dots. We saw, that by having the two dots not equal in widths the binding and anti binding states itself were really confined in either dot. This makes it a well defined qubit [2].

This indicates that the electron well widths should not be the same size. We could also see that the g parameter should be high, and the width of the hole well should be large. But if the hole well width was increased too heavily the overlap would start to drop, which of course is not optimal. Making the overlap as good as possible is one of the key components in having a effective and fast quantum gate, which leads to an effective and fast quantum computer.

Bibliography

[1] Stephen M Barnett. *Quantum Information*. Oxford, 2014 edition, 2009.

[2] David P DiVincenzo and Others. The physical implementation of quantum computation. *Fortschritte der Phys.*, 48:771–783, 2000.

[3] a. De and Craig E. Pryor. Predicted band structures of III-V semiconductors in the wurtzite phase. *Phys. Rev. B - Condens. Matter Mater. Phys.*, 81(May), 2010.

[4] J. M. Elzerman and R. Hanson. Single-shot read-out of an individual electron spin in a quantum dot. *Nature*, 430(July):431–435, 2004.

[5] Filippo Troiani, Elisa Molinari, and Ulrich Hohenester. High-finesse optical quantum gates for electron spins in artficial molecules. *Phys. Rev. Lett.*, 90(May):206802, 2003.

[6] K Bergmann, H Theuer, and B W Shore. Coherent population transfer among quantum states of atoms and molecules. *Rev. Mod. Phys.*, 70(3):1003–1023, 1998.

[7] Leslie E Ballentine. *Quantum Mechanics: A Modern Development*. World Scientific, 2010 edition, 1998.

[8] Christopher C. Gerry and Peter L. Knight. *Introductory Quantum Optics*. 2005.

[9] P.G Di Stefano and E. Paladino. Design of a lambda configuration in artificial coherent nanostructures. (c), 2015.

[10] U Gaubatz and S Schiemann. Population switching between vibrational levels in molecular beams. 149(September), 1988.

[11] J. R. Kuklinski, U. Gaubatz, F. T. Hioe, and K. Bergmann. Adiabatic population transfer in a three-level system driven by delayed laser pulses. *Phys. Rev. A*, 40(11):6741–6744, 1989.

[12] F.T Hioe. Linear and nonlinear constants of motion for two-photon processes in three-level systems. 29(6):0–2, 1984.

[13] B. E. King. Angular Momentum Coupling and Rabi Frequencies for Simple Atomic Transitions. 2008.

[14] Z. Kis and F. Renzoni. Qubit Rotation by STIRAP. 65:4, 2003.

[15] Charles Kittel. *Introduction to Solid State Physics*. Wiley, 7th edition, 1996.

[16] Filippo Troiani, Ulrich Hohenester, and Elisa Molinari. Electron-hole localization in coupled quantum dots. 65:11, 2002.

[17] Garnett W. Bryant and W. Jaskolski. Electronic structure of quantum-dot molecules and solids. *Phys. E Low-Dimensional Syst. Nanostructures*, 13(MARCH 2002):293–296, 2002.

[18] M Ciurla, J Adamowski, B Szafran, and S Bednarek. Modelling of confinement potentials in quantum dots. 15:261–268, 2002.

[19] Mark Fox. *Optical Properties of Solids*. 2010.

[20] C David Sherrill. An Introduction to Configuration Interaction Theory. *Technology*, 1995.

[21] Erwin Schrödinger. Quantisierung_als_Eigenwertproblem_(Dritte_Mitteilung).pdf, 1926.

[22] M. Abramowith and I. A. Stegun. *Hanbook of Mathematical Functions*. Department of Commerce, USA., 10th editi edition, 1972.

[23] Taken From. http://www.dplot.com/functions/besselj.png.

[24] H Haug and S. W Koch. *Quantum Theory of the Optical and Electronic Properties of Semiconductors*. 1990.

Appendix A

Elaborated calculations

A.1 Solving the Schrödinger equation

We now take a look at a quantum system which consists of a double well potential in the z-direction while having a potential in the radial direction approximated as a parabolic potential.

A.1.1 The Hamiltonian operator

The Hamilton operator consists of the different types of energy in the observed system. Energy comes from a kinetic and potential contribution.

The kinetic contribution is written as

$$E_{kin} = -\frac{\hbar^2}{2m_j}\nabla^2 \tag{A.1}$$

Where $j \in e \vee h$,for the electrons or holes. There is a different contribution in potential energy when looking in the z-direction and in the radial direction. In this system we have a double well potential when looking in the z-direction, $V_z = V_{DW}(z)$. In the radial direction we assume the potential to be parabolic.

$$V_r = \frac{1}{2}m_j\omega^2(x^2 + y^2)$$

This defines the Hamiltonian:

$$H = E_{kin} + V_z + V_r = -\frac{\hbar^2}{2m_j}\nabla^2 + V_{DW}(z) + \frac{1}{2}m_j\omega^2(x^2 + y^2) \tag{A.2}$$

Schrödinger's equation takes the form:

$$H\psi(x,y,z) = E\psi(x,y,z)$$

$$\left(-\frac{\hbar^2}{2m_j}\nabla^2 + V_{DW}(z) + \frac{1}{2}m_j\omega^2(x^2 + y^2)\right)\psi(x,y,z) = E\psi(x,y,z) \tag{A.3}$$

A.1.2 Separated solution for the z-direction

We assume that there exists solutions of the wave function that takes the form:

$$\psi(x, y, z) = R(x, y)Z(z) \tag{A.4}$$

The goal is to separate the Radial- and z-direction of the wave function on each side of the equation.

$$\left(-\frac{\hbar^2}{2m_j}\nabla^2 + V_{DW}(z) + \frac{1}{2}m_j\omega^2(x^2 + y^2)\right) R(x, y)Z(z) = ER(x, y)Z(z) \tag{A.5}$$

$$\left(-\frac{\hbar^2}{2m_j}\nabla_T^2 + \frac{1}{2}m_j\omega^2(x^2 + y^2)\right) R(x, y)Z(z) + \left(-\frac{\hbar^2}{2m_j}\frac{\partial^2}{\partial z^2} + V_{DW}(z)\right) R(x, y)Z(z) = ER(x, y)Z(z) \tag{A.6}$$

Where the transverse laplacian is given by $\nabla_T^2 = \frac{\partial^2}{\partial x^2} + \frac{\partial^2}{\partial y^2}$. Now both sides are divided by $R(x, y)Z(z)$, and the z and radial dependence are separated.

$$-\frac{\hbar^2}{2m_j}\frac{1}{R(x, y)}\nabla_T^2 R(x, y) + \frac{1}{2}m_j\omega^2(x^2 + y^2) - \frac{\hbar^2}{2m_j}\frac{1}{Z(z)}\frac{\partial^2}{\partial z^2}Z(z) + V_{DW}(z) = E \tag{A.7}$$

$$-\frac{\hbar^2}{2m_j}\frac{1}{Z(z)}\frac{\partial^2}{\partial z^2}Z(z) + V_{DW}(z) = E + \frac{\hbar^2}{2m_j}\frac{1}{R(x, y)}\nabla_T^2 R(x, y) - \frac{1}{2}m_j\omega^2(x^2 + y^2) \tag{A.8}$$

Now the variables are separated on each side of the equality. This means that eq. A.8 must be equal to a constant we call it, say E_z. The reasoning for this will be clear later.

$$-\frac{\hbar^2}{2m_j}\frac{1}{Z(z)}\frac{\partial^2}{\partial z^2}Z(z) + V_{DW}(z) = E_z \tag{A.9}$$

A.1.3 Analytical approach for solving the energy in the z-direction

When solving the wave function in the z-direction, the system to be considered is in this case a double well potential. This potential consists of two quantum dots placed symmetrically about the center, as seen in figure A.1.
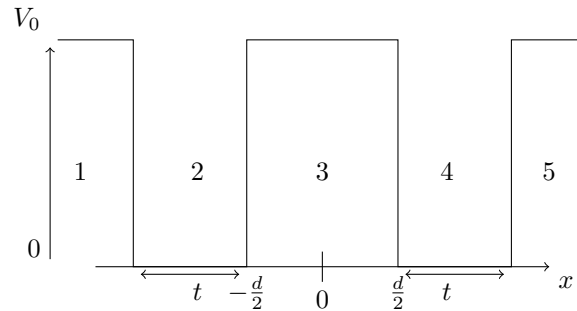

Figure A.1: Double well potential, in the z-direction

To solve the wave function we have to solve Schrödinger's equation in the 5 regions also shown in figure A.1. The potential in this system to be considered has the following form:

$$V(z) = \begin{cases} V_0 & z < -\frac{d}{2} - t \\ 0 & -\frac{d}{2} - t < z < -\frac{d}{2} \\ V_0 & -\frac{d}{2} < z < \frac{d}{2} \\ 0 & \frac{d}{2} < z < \frac{d}{2} + t \\ V_0 & \frac{d}{2} + t < z \end{cases} \tag{A.10}$$

Schrödinger's equation therefore takes two forms:

For $V = 0$

$$-\frac{\hbar^2}{2m_e} \frac{\partial^2}{\partial z^2} Z(z) = E_z Z(z) \tag{A.11}$$

For $V = V_0$

$$-\frac{\hbar^2}{2m_e} \frac{\partial^2}{\partial z^2} Z(z) = (E_z - V_0) Z(z) \tag{A.12}$$

Now these two should be solved in their respective areas.

For $z < -\frac{d}{t} - t$, and potential $V = V_0$:

Here $V_0 > E_z > 0$ which means the states are bounded.

$$\frac{\partial^2}{\partial z^2} Z(z) = \kappa^2 Z(z) \tag{A.13}$$

Where κ of course is given by

$$\kappa = \frac{\sqrt{(V_0 - E_z)2m_e}}{\hbar} \tag{A.14}$$

This is an easily solvable differential equation, which gives the solution:

$$Z(z) = A' \exp\left(-\kappa z\right) + A \exp\left(\kappa z\right) \tag{A.15}$$

since the first term blows up by tending to infinity as $z \to -\infty$ this is not a solution and we end up with:

$$Z(z) = A \exp\left(\kappa z\right) \tag{A.16}$$

For $-\frac{d}{2} - t < z < -\frac{d}{2}$, and potential $V = 0$:

In this region Schrödinger's equation takes the form:

$$\frac{\partial^2}{\partial z^2} Z(z) = -l^2 Z(z) \tag{A.17}$$

where we define that constant l as:

$$l = \frac{\sqrt{E_z 2m_e}}{\hbar} \tag{A.18}$$

This gives the solution to the differential equation:

$$Z(z) = B \sin\left(lz\right) + B' \cos\left(lz\right) \tag{A.19}$$

For $-\frac{d}{2} < z < \frac{d}{2}$, and potential $V = V_0$:

This yields the same solution as in region 1:

$$Z(z) = C \exp\left(-\kappa z\right) + C' \exp\left(\kappa z\right) \tag{A.20}$$

Due to the symmetry of the system, the constants in this region must be either equal (bonding) or have sign change i.e. $C = C'$ for the bonding states and $C = -C'$ for the anti-bonding states. We can rewrite the expression:

$$Z(z)_b = C\left(\exp\left(-\kappa z\right) + \exp\left(\kappa z\right)\right) = 2C\cosh\left(\kappa z\right) \tag{A.21}$$

$$Z(z)_{ab} = 2C\sinh\left(\kappa z\right) \tag{A.22}$$

In principle we could have solved it by not taking any symmetry into consideration, but in the end it would yield the same result.
The last two regions yields almost the same solutions. The term that blows up in region 5 is instead $A' \exp\left(\kappa z\right)$ which gives the solutions:
For $\frac{d}{2} < z < \frac{d}{2} + t$, and potential $V = 0$:

$$Z(z) = B \sin\left(lz\right) + B' \cos\left(lz\right) \tag{A.23}$$

For $\frac{d}{2} + t < z$, and potential $V = V_0$:

$$Z(z) = A \exp\left(-\kappa z\right) \tag{A.24}$$

A.1.4   Boundary conditions for the z-dependant wave function

The next step into solving the wave function in the z-direction is to apply boundary conditions between the regions in order to solve the constants A, B, B' and C. Here we solve for the bonding states. There are two boundary conditions that the regions have to obey in the boundary between them:

$$\psi_1(x_0) = \psi_2(x_0) \tag{A.25}$$

$$\frac{d\psi_1(x_0)}{dx} = \frac{\psi_2(x_0)}{dx} \tag{A.26}$$

Because of the symmetry in the system, we only have to solve the boundary conditions in the first two boundaries, to solve the constants. To do this we apply Cramer's rule. The matrix of the system consists of the boundary conditions, where the two first rows are from eq. A.25 and the last row are from eq. A.26 in the first boundary . We solve constants B, B' and C so they all depend on A which later is solved by normalization of the wave function. The matrix for B, B' and C takes the form:

$$M = \begin{bmatrix} 2\cosh\left(\frac{d}{2}\kappa\right) & -\sin\left(\frac{d}{2}l\right) & -\cos\left(\frac{d}{2}l\right) \\ 0 & \exp\left(\left(\frac{d}{2}+t\right)\kappa\right)\cdot\sin\left(\left(\frac{d}{2}+t\right)l\right) & \exp\left(\left(\frac{d}{2}+t\right)\kappa\right)\cdot\cos\left(\left(\frac{d}{2}+t\right)l\right) \\ 0 & \exp\left(\kappa\left(\frac{d}{2}+t\right)\right)\cdot l\cos\left(l\left(\frac{d}{2}+t\right)\right) & -\exp\left(\kappa\left(\frac{d}{2}+t\right)\right)\cdot l\sin\left(l\left(\frac{d}{2}+t\right)\right) \end{bmatrix}$$

We call the determinant of the matrix that describes the system $D = \det M$. We then need the matrices where the B, B' and C columns are removed respectively, and replaced with the column vector for A instead

$$A = \begin{bmatrix} 0 \\ A \\ 0 \end{bmatrix} \tag{A.27}$$

we call these 3 matrices M_B, $M_{B'}$ and M_C. We take the determinant of each of these matrices:

$$D_B = \det M_B \tag{A.28}$$

$$D_{B'} = \det M_{B'} \tag{A.29}$$

$$D_C = \det M_C \tag{A.30}$$

By Cramer's rule we can solve B, B' and C, only depending on A by:

$$B = \frac{D_B}{D} \tag{A.31}$$

$$B' = \frac{D_{B'}}{D} \tag{A.32}$$

$$C = \frac{D_C}{D} \tag{A.33}$$

Now the wave function needs to be normalized which is done by $\int_{-\infty}^{\infty} |Z(z)|^2 dz = 1$, and the last constant A is obtained.

The energy is solved by numerical methods, exploiting the boundary condition in eq. A.26. Here we solve for the boundary at $\frac{d}{2}$, this yields:

$$2C\kappa \sinh\left(\kappa\frac{d}{2}\right) = Bl \cos\left(l\frac{d}{2}\right) - B'l \sin\left(l\frac{d}{2}\right) \tag{A.34}$$

$$\frac{2C\kappa \sinh\left(\kappa\frac{d}{2}\right) + B'l \sin\left(l\frac{d}{2}\right)}{B} = l \cos\left(l\frac{d}{2}\right) \tag{A.35}$$

The left hand side and right hand side of eq. A.35 are plotted as a function of energy, the solutions for the energy will be the crossings between the two graphs. The result can be seen in figure A.2a, which shows the 3 first solutions corresponding to the ground sate, first and second excited states for the bonding state. Figure A.2b shows the 3 lowest energies for the anti bonding state. The ground state for the system as a whole, is the first energy of the bounded state. The first exited state for the system is the first energy for the anti bonding state.

These discrete values of energy now enable us to plot the wave function corresponding to the chosen energy level. The plotted wave function for the bonding ground state can be seen in figure A.3a. The wave function for the anti bonding ground state, can be seen in figure A.3b.
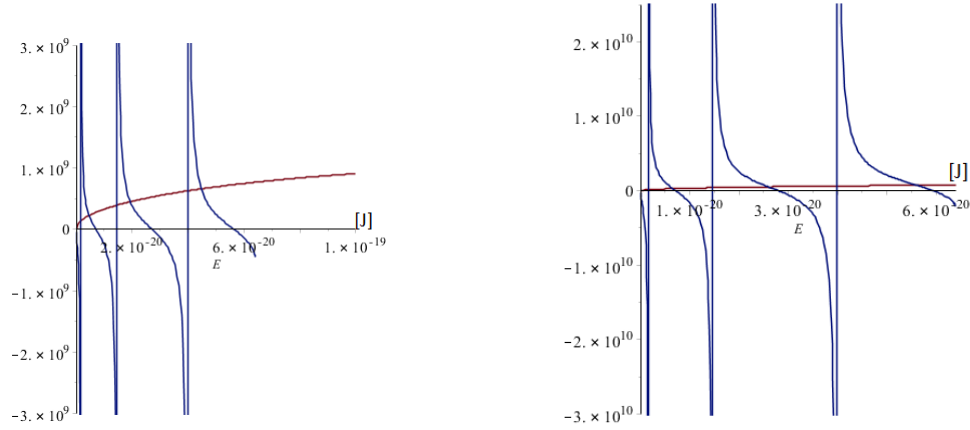
(a) Energy of the bonding states in the z-direction *(b)* Energy of the anti bonding states in the z-direction

Figure A.2: Bonding and anti bonding energies in the z-direction
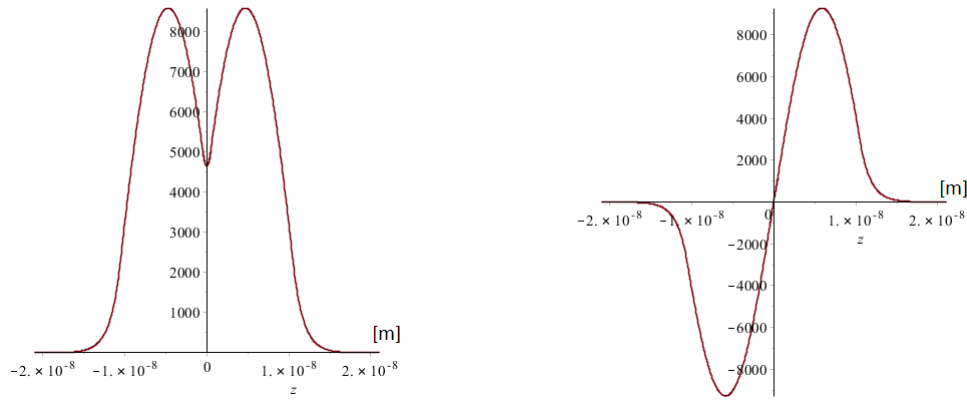
(a) Bonding ground state wave function in the z-direction *(b)* Anti bonding ground state wave function in the z-direction

Figure A.3: Bonding and anti bonding wave functions for the ground state

A.1.5 Separated solution for the radial direction

From eq. A.8 we can separate the radial dependent part and we get

$$-\frac{\hbar^2}{2m_j}\nabla_T^2 R(x,y) + \frac{1}{2}m_j\omega^2(x^2+y^2)R(x,y) = (E-E_z)R(x,y) \qquad (A.36)$$

Before solving this, we introduce the dimensionless scaling factors [21]:

$$b = \left(\frac{\hbar}{m_e\omega}\right)^{\frac{1}{2}}, \quad W = \frac{E-E_z}{\hbar\omega} \qquad (A.37)$$

And also the dimensionless polar coordinates:

$$x = br\cos\left(\theta\right), \quad y = br\sin\left(\theta\right) \qquad (A.38)$$

The standard Laplace operator in cartesian coordinates is given by:

$$\nabla_T^2 = \frac{d^2}{dx^2} + \frac{d^2}{dy^2} \qquad (A.39)$$

we want to rewrite this as derivatives of the distance r and angle θ instead. From the dimensionless polar coordinates we have:

$$x = br\cos(\theta), \quad y = br\sin(\theta) \tag{A.40}$$

These 2 equations can be rewritten so we have the following:

$$r = \frac{\sqrt{x^2 + y^2}}{br}, \quad \cos(\theta) = \frac{x}{\sqrt{x^2 + y^2}}, \quad \sin(\theta) = \frac{y}{\sqrt{x^2 + y^2}} \tag{A.41}$$

by adding the two equations in A.40 to find the expression for r, and then substituting r in both of the dimensionless polar coordinates to get an expression for $\cos(\theta)$ and $\sin(\theta)$.

The differential operators can be computed via the chain rule which gives us:

$$\frac{d}{dx} = \frac{dr}{dx}\frac{d}{dr} + \frac{d\theta}{dx}\frac{d}{d\theta}, \quad \frac{d}{dy} = \frac{dr}{dy}\frac{d}{dr} + \frac{d\theta}{dy}\frac{d}{\theta} \tag{A.42}$$

To calculate the r dependences is straight forward:

$$\frac{dr}{dx} = \frac{d}{dx}\frac{\sqrt{x^2 + y^2}}{b} = \frac{\cos(\theta)}{b}, \quad \frac{dr}{dy} = \frac{d}{dy}\frac{\sqrt{x^2 + y^2}}{b} = \frac{\sin(\theta)}{b} \tag{A.43}$$

Next we compute $\frac{dx}{d\theta}$, this gives:

$$\frac{dx}{d\theta} = b\left(\cos(\theta)\frac{dr}{d\theta} - r\sin(\theta)\right) \tag{A.44}$$

$$dx = b\left(\cos(\theta)\,dr - r\sin(\theta)\,d\theta\right) \tag{A.45}$$

$$-\sin(\theta)\,d\theta = \frac{dx}{br} - \frac{\cos(\theta)\,dr}{r} \tag{A.46}$$

From equation A.43 we can write $dr = \frac{\cos(\theta)}{b}dx$, which gives us:

$$\frac{dx}{br} - \frac{\cos(\theta)\,dr}{r} = \left(\frac{1}{br} - \frac{\cos(\theta)}{r}\frac{\cos(\theta)}{b}\right)dx = \left(1 - \cos(\theta)^2\right)\frac{dx}{br} = \frac{\sin(\theta)^2}{br}dx \tag{A.47}$$

This gives us the equation:

$$-\sin(\theta)\,d\theta = \frac{\sin(\theta)^2}{br}dx \tag{A.48}$$

$$\frac{d\theta}{dx} = -\frac{\sin(\theta)}{br} \tag{A.49}$$

The same calculations can be done with dy and this in the end yields:

$$\frac{d\theta}{dy} = \frac{\cos(\theta)}{br} \tag{A.50}$$

We can now write the the terms for $\frac{d}{dx}$ and $\frac{d}{dy}$:

$$\frac{d}{dx} = \frac{\cos(\theta)}{b}\frac{d}{dr} - \frac{\sin(\theta)}{rb}\frac{d}{d\theta}, \quad \frac{d}{dy} = \frac{\sin(\theta)}{b}\frac{d}{dr} + \frac{\cos(\theta)}{rb}\frac{d}{dr} \tag{A.51}$$

By insertion of $\frac{d}{dx}$ and $\frac{d}{dy}$ into $\nabla_T^2 = \frac{d^2}{dx^2} + \frac{d^2}{dy^2}$, by computing $\frac{d^2}{dx^2}$ and $\frac{d^2}{dy^2}$ this yields:

$$\nabla_T^2 = \frac{d^2}{dx^2} + \frac{d^2}{dy^2} \tag{A.52}$$

$$= \left(\cos(\theta)^2 + \sin(\theta)^2\right)\frac{1}{b^2}\frac{d^2}{dr^2} + \left(\cos(\theta)^2 + \sin(\theta)^2\right)\frac{1}{b^2r}\frac{d}{dr} + \left(\cos(\theta)^2 + \sin(\theta)^2\right)\frac{1}{r^2b^2}\frac{d^2}{d\theta^2} \tag{A.53}$$

$$= \frac{1}{b^2}\frac{d^2}{dr^2} + \frac{1}{b^2r}\frac{d}{dr} + \frac{1}{r^2b^2}\frac{d^2}{d\theta^2} \tag{A.54}$$

This yields the final result for the Laplace operator in the transverse direction in polar coordinates:

$$\nabla_T^2 = \frac{1}{b^2}\frac{d^2}{dr^2} + \frac{1}{b^2r}\frac{d}{dr} + \frac{1}{r^2b^2}\frac{d^2}{d\theta^2} \tag{A.55}$$

The transverse Laplace operator can now be written as:

$$\nabla_T^2 = \frac{1}{b^2}\frac{d^2}{dr^2} + \frac{1}{b^2r}\frac{d}{dr} + \frac{1}{r^2b^2}\frac{d^2}{d\theta^2} \tag{A.56}$$

This result for the transverse Laplace operator, can now be used to solve the Schrödinger equation for the radial part, it yields the following:

$$\frac{1}{b^2}\left(\frac{d^2}{dr^2} + \frac{1}{r}\frac{d}{dr} + \frac{1}{r^2}\frac{d^2}{d\theta^2}\right)R(r,\theta) + \left(\frac{2m_e\omega}{\hbar}W - \frac{m_e\omega}{\hbar}r^2\right)R(r,\theta) = 0 \tag{A.57}$$

$$\left(\frac{d^2}{dr^2} + \frac{1}{r}\frac{d}{dr} + \frac{1}{r^2}\frac{d^2}{d\theta^2}\right)R(r,\theta) + b^2\left(\frac{2m_e\omega}{\hbar}W - \frac{m_e\omega}{\hbar}r^2\right)R(r,\theta) = 0 \tag{A.58}$$

$$\left(\frac{d^2}{dr^2} + \frac{1}{r}\frac{d}{dr} + \frac{1}{r^2}\frac{d^2}{d\theta^2}\right)R(r,\theta) + (2W - r^2)R(r,\theta) = 0 \tag{A.59}$$

The potential is assumed to be rotational symmetric in the radial direction, and the solution of the wave function then takes the form:

$$R(r,\theta) = \exp(im\theta)\,R(r) \tag{A.60}$$

We insert this in the solution and reduce it to get:

$$\frac{d^2}{dr^2}R(r) + \frac{1}{r}\frac{d}{dr}R(r) + \left(2W - \frac{m^2}{r^2} - r^2\right)R(r) = 0 \tag{A.61}$$

We now substitute $\rho = r^2$ and use the chain rule to get $\frac{d}{dr} = \frac{d\rho}{dr}\frac{d}{d\rho} = 2r\frac{d}{d\rho}$. This gives us :

$$\frac{d^2}{d\rho^2}R(r) + \frac{1}{\rho}\frac{d}{d\rho}R(r) + \left(\frac{W}{2\rho} - \frac{m^2}{4\rho^2} - \frac{1}{4}\right)R(r) = 0 \tag{A.62}$$

This type of equation is already solved in Schrödinger's article, and the solution is also found in Abramowitz and Stegun[22]. The eigenfunction is given by:

$$R(r)_{m,k} = r^n \exp\left(-\frac{r^2}{2}\right)L_k^m(r^2) \tag{A.63}$$

$$P(r, \theta) = r^n \exp\left(-\frac{r^2}{2}\right) L_k^m(r^2) \exp(im\theta) \tag{A.64}$$

This solution is not yet normalized.
The eigenvalues for the eigenfunction are $W = 2k + m + 1$, or in general:

$$2k + m + 1 = \frac{(E - E_z)}{\hbar\omega} \tag{A.65}$$

A.1.6 Analytical approach for solving the energy in the radial-direction

In the radial direction, the system to be considered is a simple parabolic potential. The wave function is solved in the radial direction, so it is possible to obtain the energies for the wave function. The eigenvalues are given by $2k + m + 1 = \frac{(E-E_z)}{\hbar\omega}$, which tells us that the ground state has the eigenvalues $k = 0$, $m = 0$ while the first exited state has $k = 0$, $m = 1$ and so forth.

(a) Radial wave function for $m = 0, k = 0$

(b) Radial wave function for $m = 1, k = 0$
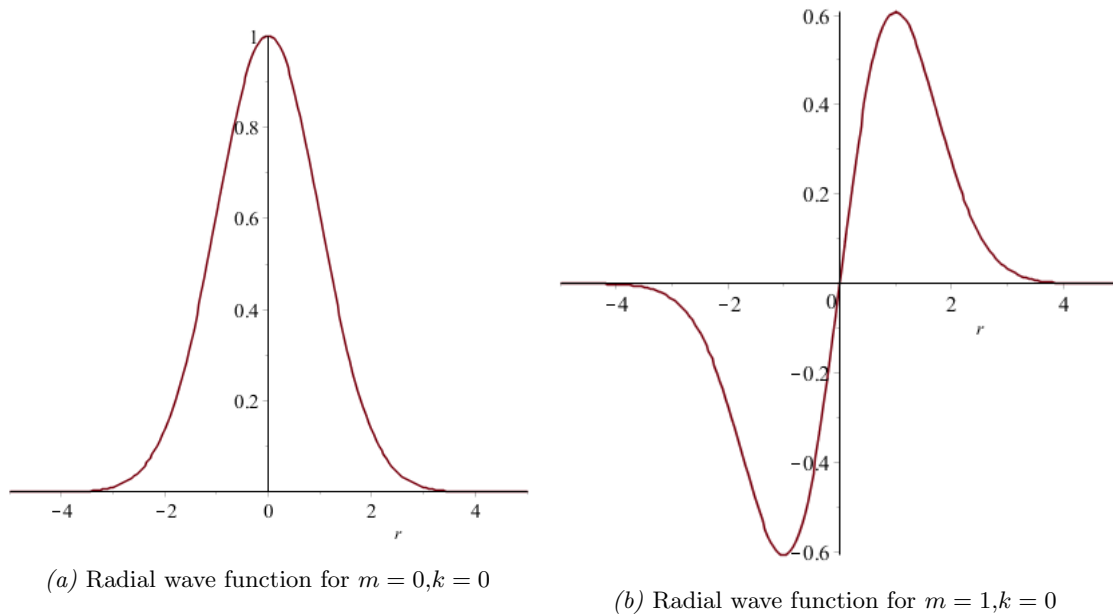
Figure A.4: The ground state and first exited state of the radial wave function

Figure A.4 shows the first two states of the radial wave function for a fixed angle.

A.1.7 Nanowire with spherical infinite potential in the radial direction

The system to be considered now, is instead of a parabolic potential, a wire with infinite potential at the boundaries and with zero potential inside the wire:

$$V(r) = \begin{cases} \infty & r > r_{wire} \\ 0 & r \leq r_{wire} \end{cases} \tag{A.66}$$

Assuming that the Schrödinger equation can be separated by variables we get the equation in the radial direction

$$-\frac{\hbar}{2m_e}\nabla_T^2\psi_T = (E - E_z)\psi_T \tag{A.67}$$

The transverse Laplace operator is given by:

$$\nabla_T^2 = \frac{\partial^2}{\partial r^2} + \frac{1}{r}\frac{\partial}{\partial r} + \frac{1}{r^2}\frac{\partial^2}{\partial \theta^2} \tag{A.68}$$

Since the potential is assumed to be rotational symmetric we can write the wave function as $\psi_T = R(r)\exp{(in\theta)}$ and thus by the separated Schrödinger equation

$$-\frac{\hbar^2}{2m_e}\left(\frac{\partial^2}{\partial r^2}R(r) + \frac{1}{r}\frac{\partial}{\partial r}R(r) + \frac{R(r)}{r^2}\frac{\partial^2}{\partial \theta^2}\right)\exp{(in\theta)} = (E - E_z)R(r)\exp{(in\theta)} \tag{A.69}$$

$$-\frac{\hbar^2}{2m_e}\left(\frac{\partial^2}{\partial r^2}R(r) + \frac{1}{r}\frac{\partial}{\partial r}R(r) - \frac{n^2}{r^2}R(r)\right) - (E - E_z)R(r) = 0 \tag{A.70}$$

$$r^2\frac{\partial^2}{\partial r^2}R(r) + r\frac{\partial}{\partial r}R(r) + \left(\frac{2m_e}{\hbar^2}(E - E_z)r^2 R(r) - n^2 R(r)\right) = 0 \tag{A.71}$$

The solution to this differential equation can be found in Abramowitz and Stegun[22], and gives the following solution:

$$R(r) = (J_n + Y_n + H_n^{(1)} + H_n^{(2)})(\lambda r) \tag{A.72}$$

Since $Y_n(x)$, $H_n^{(1)}(x)$ and $H_n^{(2)}(x) \to \infty$ for $x \to 0$ we are left with the Bessel function $J_n(x)$ so our solution ends up being

$$R(r) = AJ_n(\lambda r) \tag{A.73}$$

Where A is the normalization constant and λ is given by

$$\lambda = \sqrt{\frac{2m_e}{\hbar^2}(E - E_z)} \tag{A.74}$$

Thus the wavefunction is

$$\psi_T = AJ_n(\lambda r)\exp{(in\theta)} \tag{A.75}$$

A.1.8   Boundary condition for the nanowire with infinite potential in the radial direction

The infinite potential at the boundary of the nanowire gives us the boundary condition

$$R(r) \to 0, \quad r \to r_{wire} \tag{A.76}$$

Where r_{wire} is the radius of the nanowire. This tells us that:

$$R(r_{wire}) = AJ_n(\lambda r_{wire}) = 0 \tag{A.77}$$

which implies that the Bessel function has to be equal to zero

$$J_n(\lambda r_{wire}) = 0 \tag{A.78}$$

The Bessel function is equal to zero, for arguments that are determined numerically.
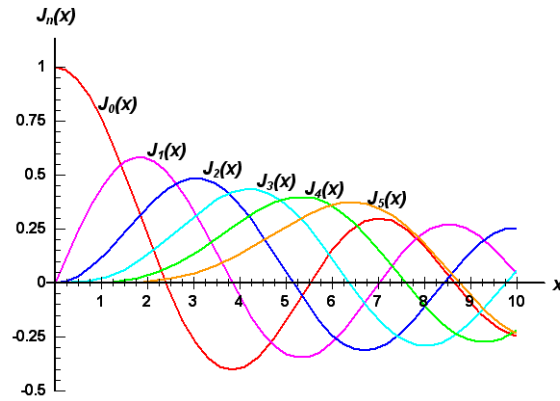
Figure A.5: First couple of Bessel functions [23]

The lowest energy is therefore at the first Bessel function zero for $J_0(x)$ which is $x = 2.4048$ i.e. the ground state energy can be found from solving the expression $(E - E_z)$ in:

$$2.4048 = \sqrt{\frac{2m_e}{\hbar^2}(E - E_z)} \cdot r_{wire} \tag{A.79}$$

The first exited energy can then be found from the first zero for the function $J_1(x)$ the next energy is then the first zero for $J_2(x)$, and then the next energy is the second zero for $J_0(x)$ as seen on figure A.5

A.2   Cauchy's residue theorem

The residues to be evaluated is based on the Laurent series of a given function about a point z_0 which is given by:

$$f(z) = \sum_{n=-\infty}^{\infty} a_n(z - z_0)^n \tag{A.80}$$

The residue will then, due to Laurent's theorem, be equal to the constant a_{-1}, and since:

$$a_k = \frac{1}{2\pi i} \oint_C \frac{f(z)}{(z - z_o)^{k+1}} dz \tag{A.81}$$

we can find our integral to be :

$$\oint_C f(z)dz = a_{-1}2\pi i \tag{A.82}$$

so combining equation 4.13 and A.82 we can see:

$$a_{-1} \equiv \sum_{k=1}^{n} Res\left(f(z), z_k\right) \tag{A.83}$$

To evaluate a_{-1}, we expand the Laurent series, and isolate a_{-1} since this constant is the one where the term shifts from getting divided by $(z - z_0)$ to getting multiplied

by $(z - z_0)$ and this being the highest order constant which contains the divergence. This is done by multiplying each side of the Laurent series with $(z - z_0)^n$

$$f(z) = \frac{a_{-n}}{(z - z_0)^n} + ... + \frac{a_{-1}}{(z - z_0)} + a_0 + a_1(z - z_0) + ...a_n(z - z_0)^n \qquad (A.84)$$

$$(z - z_0)^n f(z) = a_{-n} + .. + a_{-1}(z - z_0)^{n-1} + a_0(z - z_0)^n + ...a_n(z - z_0)^{2n} \qquad (A.85)$$

This term is then differentiated n-1 times to make all the lower order terms cancel out:

$$\frac{d^{n-1}}{dz^{n-1}}(z - z_0)^n f(z) = (n - 1)!a_{-1} + a_0(z - z_0) \qquad (A.86)$$

To isolate a_{-1} , the term is just divided by $(n - 1)!$ and then let $z \to z_0$

$$a_{-1} = \frac{1}{(n - 1)!} \lim_{z \to z_0} \frac{d^{n-1}}{dz^{n-1}}(z - z_0)^n f(z) = Res\,(f(z), z_0) \qquad (A.87)$$

Here n is the order of the pole when $f(z)$ has been factorized, and z_0 is the point of the pole. In equation 4.13 , we see it is a sum over all residues. This is due to Cauchy's theorem which tells us that a function integrated over an area with no divergences inside must be equal to zero, the function itself can still have divergences tough.

$$\oint_\gamma f(z)dz = 0 \qquad (A.88)$$

Since there are 1 or more divergences when using the residual theorem we get a sum over all the integrals containing a divergence, since the rest of the integral is just equal to zero:

$$\oint_C = \oint_{c1} + \oint_{c2} + ... = \sum_{k=1}^{n} Res\,(f(z), z_k)) \qquad (A.89)$$

And this proves Cauchy's Residue theorem.

A.3 Convergence of the riemann sum

There are some details about creating the riemanns sums which differ depending on what implementation is used. In this case a vector from the startpoint to the endpoint in steps of the stepsize is created. Letting the function to be integrated take this vector as input and multiplying the result with the the step size and finally summing this will give the approximate area under the curve. However the step size will not always match the endpoints completely, and as such the stepsize needs to be corrected a bit such that an integer number of steps from start to end can be made in each region, otherwise the convergence is not uniform. When this is done one notes that, since this is a left hand sum, the sum gets a "bar" of delta x too much in the area because it evaluates the function at a point and multiplies this with a step size, moves on one step size, evaluates the function and so on, up until evaluating the endpoint times the step size whereafter it stops. On figure A.6 is a left hand sum, where the startpoint is x_0 and the endpoint is x_3 in this implementation. Therefore one needs to subtract one stepsize from the endpointvalue in order to obtain the

---

[1]From `http://upload.wikimedia.org/wikipedia/commons/c/cc/Riemann_Sum_Left_Hand.png`
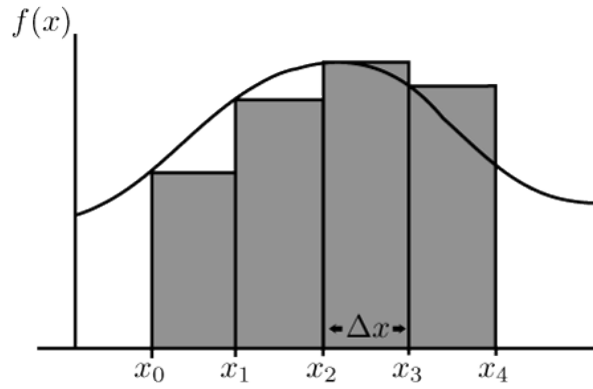
Figure A.6: [1]Depiction of a left hand sum

correct result, otherwise the result will always be an extra stepsize times function value in the endpoint too large. The effects of not making these corrections are plotted in figure A.7.

$$f(x) = 1 \qquad\qquad\qquad f(x) = 1 + \sin(x)$$
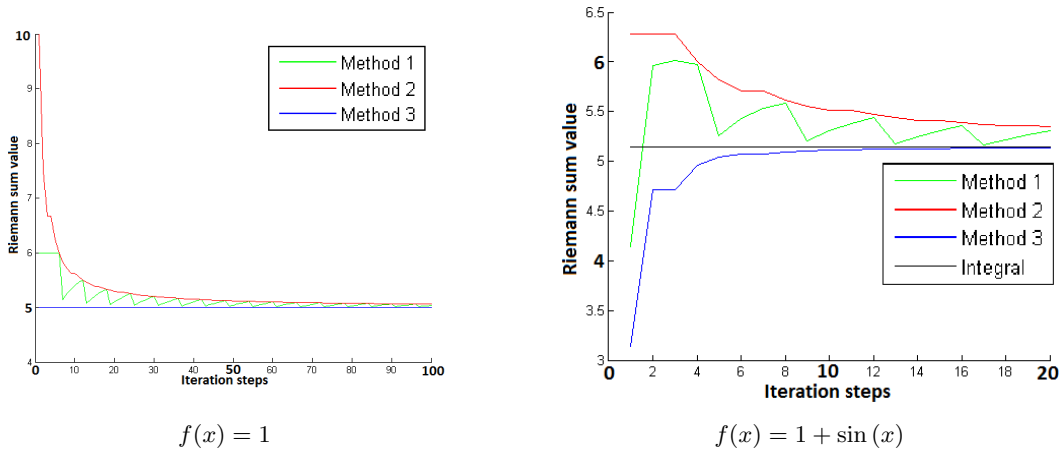
Figure A.7: The approximated integral over two chosen functions with the number of iteration steps on the abscissa. Method 1 is when the stepsize is not scaled with the interval, Method 2 is when the last "bar" is not subtracted, Method 3 is the correct implementation of the riemann sum approximation. (The reason for the green curve being less than the correct value in the first iteration in the righthand figure, and not greater than as would have been expected, is a technical detail of the first step size being greater than the considered interval.)

A.4   Dipole-element in a periodic potential

We wish to calculate the dipole-moment between two electrons, since this describes the probability of transition. The dipole-element is in general given by:

$$\mathbf{D} = \langle \Psi_1 | \mathbf{r}\Psi_2 \rangle \tag{A.90}$$

For a periodic potential a wave function can be written as:

$$\Psi(\mathbf{r}) = u(\mathbf{r})F(\mathbf{r}) \tag{A.91}$$

This is due to Bloch's theorem, which states that a wave function in a periodic potential can be written as a periodic function $u(\mathbf{r})$ such that $u(\mathbf{r+R}) = u(\mathbf{r})$, where $\mathbf{R}$ is a lattice vector, times the envelope function $F(\mathbf{r})$, which describes the envelope of a given wave function. The dipole-moment for a periodic potential can then be written as:

$$\mathbf{D} = \langle\Psi_1|\mathbf{r}\Psi_2\rangle = \langle u_1 F_1|u_2 F_2\rangle = \int F_1^*(\mathbf{r})F_2(\mathbf{r})u_1^*(\mathbf{r})\mathbf{r}u_2(\mathbf{r})d\mathbf{r} \tag{A.92}$$

We now assume via the envelope approximation that F varies slow so it cna be assumed to be constant. Then we sum up and integrate over all unit cells of index i, which gives us a new expression for the dipole-moment:

$$\mathbf{D} = \sum_i F_{1,i}^* F_{2,i} \int_{uc,i} u_1^*(\mathbf{r})\mathbf{r}u_2(\mathbf{r})d\mathbf{r} \tag{A.93}$$
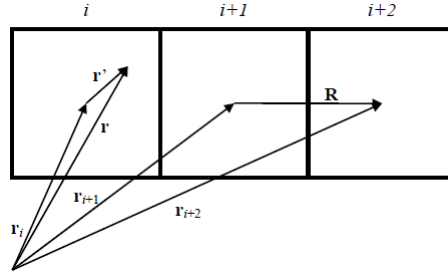
Figure A.8: Vectors in a unit cell i, and the lattice vector R

As seen in figure A.8, the vector $\mathbf{r}$ can be written as $\mathbf{r} = \mathbf{r}_i + \mathbf{r}'$, and since $u(\mathbf{r})$ is periodic we have that $u(\mathbf{r}_1 + \mathbf{r}') = u(\mathbf{r}_j + \mathbf{r}')$ where i and j are different unit cells. The integral that is equal to the dipole moment can then be written on the form:

$$\mathbf{D} \cong \langle u_1|u_2\rangle \int F_1^*(\mathbf{r})F_2(\mathbf{r})\mathbf{r}d\mathbf{r} + \langle u_1|\mathbf{r}'u_2\rangle \int F_1^*(\mathbf{r})F_2(\mathbf{r})\mathbf{r}d\mathbf{r} \tag{A.94}$$

Because of the symmetry in the system, the two inner products can be evaluated in terms of being zero or non zero. They are dependent on whether the transition is an interband transition i.e. the transition is happening between the valence band and conduction band or if it is intraband i.e. happening between two states in the same band. The symmetry gives:

$$\langle u_1|u_2\rangle = 0 \quad \text{(interband)} \tag{A.95}$$

$$\langle u_1|\mathbf{r}'u_2\rangle = 0 \quad \text{(intraband)} \tag{A.96}$$

The transition which are relevant for this system is the interband transition. Which gives us the dipole-moment as:

$$\mathbf{D} = \langle u_1|\mathbf{r}'u_2\rangle \int F_1^*(\mathbf{r})F_2(\mathbf{r}) \tag{A.97}$$

The integral $\langle u_1 | \mathbf{r}' u_2 \rangle$ is very complicated to calculate, and is often evaluated and determined experimentally. Therefore an approximation of the dipole-moment is only dependent on the two envelope functions. It is therefore enough to only optimize the integral between these two envelope functions to maximize our dipole-moment.

A.5   Coulomb matrix elements

The interaction potential can from [24] be written as

$$v(\boldsymbol{r} - \boldsymbol{r}') = \sum_{\mathbf{q}} V_{\mathbf{q}} \exp\left(i\boldsymbol{q} \cdot (\boldsymbol{r} - \boldsymbol{r}')\right) \tag{A.98}$$

with $V_{\mathbf{q}} = -\dfrac{e^2}{V \epsilon \boldsymbol{q}^2}$. A coulomb matrix element will then become:

$$\langle ij| \hat{H}_c |i'j'\rangle = \sum_{\mathbf{q}} \int d\boldsymbol{r} \psi_i^*(\boldsymbol{r}) \psi_{i'}(\boldsymbol{r}) \exp\left(i\boldsymbol{q} \cdot \boldsymbol{r}\right) \int d\boldsymbol{r}' \psi_j^*(\boldsymbol{r}) \psi_{j'}(\boldsymbol{r}') \exp\left(-i\boldsymbol{q} \cdot \boldsymbol{r}'\right) \tag{A.99}$$

The dot product between the r and q vector is $\boldsymbol{q} \cdot \boldsymbol{r} = q_r r \cos\left(\theta\right) + q_z z$. The electron part of the wavefunction is (using the angular part of the wavefunctions are a complex exponential, where we only consider i and i' with equal angular parts, and thus evaluates to unity):

$$\int d\boldsymbol{r} \psi_i^*(\boldsymbol{r}) \psi_{i'}(\boldsymbol{r}) \exp\left(i\boldsymbol{q} \cdot \boldsymbol{r}\right) \tag{A.100}$$

$$= \int dz \int dr r R_i^*(r) R_{i'}(r) Z_i(z)^* Z_{i'}(z) \exp\left(iq_z z\right) 2\pi J_0(q_r r) \tag{A.101}$$

Inserting into equation (A.99) and taking the limit of the sum over q vector going to an integral.

$$\langle ij| \hat{H}_c |i'j'\rangle = \frac{e^2}{\epsilon} \int dq_r q_r \int dq_z \int dz \int dz' \frac{\exp\left(iq_z \left(z - z'\right)\right)}{q_r^2 + q_z^2} \tag{A.102}$$

$$\times \int dr r R_i^*(r) R_{i'}(r) Z_i(z)^* Z_{i'}(z) J_0(q_r r) \int dr' r' R_j^*(r') R_{j'}(r') Z_j(z')^* Z_{j'}(z') J_0(q_r r') \tag{A.103}$$

Using cauchy's residue theorem to integrate the around the divergence in $q_z = i q_r$ for the q_z integral. The redidues are $\frac{1}{2iq_r} \exp\left(-q_r |z - z'|\right)$ and thus the integral evaluates to

$$\int dq_z \frac{\exp\left(iq_z \left(z - z'\right)\right)}{q_r^2 + q_z^2} = \frac{\pi}{q_r} \exp\left(-q_r |z - z'|\right) \tag{A.104}$$

And thus the final matrix element becomes

$$\langle ij| \hat{H}_C |i'j'\rangle = -\frac{e^2 \pi}{\epsilon} \iiint dq\,dz\,dz' \exp\left(-q |z - z'|\right) Z_i(z) Z_j(z') Z_{i'}(z) Z_{j'}(z') \tag{A.105}$$

$$\times \int dr r R_i(r) R_{i'}(r) J_0(qr) \int dr' r' R_j(r') R_{j'}(r') J_0(qr') \tag{A.106}$$

Appendix B

MatLab code

B.1 The main exciton script

```
%Script to calculate the coulomb hamiltonian on matrix form

%Distances in the z direction - d for separation distance between wells, t
%for thickness in the wells. Follows the structure described in Troiani2002
d=1e-9; t=10e-9;
hbar=1.055e-34;
m0=9.11e-31;
%Conversion factor between meV and J
omr=1.6022e-22;
%Defining necessary constants based on numerical calculations of the energy
%in the z direction.
[le,ke,ae,be,Be,Bme,Ce,Bae,Bmae,Cae,ENele]=EnergiZ('electron');
[lh,kh,ah,bh,Bh,Bmh,Ch,Bah,Bmah,Cah,ENhul]=EnergiZ('hole');
%Defining the parabolic potential frequencies.
omegaE=3.038535e13; %20meV/hbar
omegaH=5.32e12; %3.5meV/hbar
%Defining the scale factors introduced in solving the transverse potential.
bscaleEle=sqrt(hbar/(0.069*m0*omegaE));
bscaleHul=sqrt(hbar/(0.38*m0*omegaH));

kafenergi=zeros(1,4);
lafenergi=zeros(1,4);
syms r rm z zm q
%Defining the constants from the calculations of the wavefunctions.
Knst=zeros(6,5); %Knst (A, B, Bm, C, Energien | b1,b2,b3a1a2a3 osv. )
[Knst(1,1),Knst(1,2),Knst(1,3),Knst(1,4),Knst(1,5)]=zwfun('11','electron');
[Knst(2,1),Knst(2,2),Knst(2,3),Knst(2,4),Knst(2,5)]=zwfun('12','electron');
[Knst(3,1),Knst(3,2),Knst(3,3),Knst(3,4),Knst(3,5)]=zwfun('13','electron');
[Knst(4,1),Knst(4,2),Knst(4,3),Knst(4,4),Knst(4,5)]=zwfun('41','electron');
[Knst(5,1),Knst(5,2),Knst(5,3),Knst(5,4),Knst(5,5)]=zwfun('42','electron');
[Knst(6,1),Knst(6,2),Knst(6,3),Knst(6,4),Knst(6,5)]=zwfun('43','electron');
Knstm=zeros(6,5); %For the holes
[Knstm(1,1),Knstm(1,2),Knstm(1,3),Knstm(1,4),Knstm(1,5)]=zwfun('11','hole');
[Knstm(2,1),Knstm(2,2),Knstm(2,3),Knstm(2,4),Knstm(2,5)]=zwfun('12','hole');
[Knstm(3,1),Knstm(3,2),Knstm(3,3),Knstm(3,4),Knstm(3,5)]=zwfun('13','hole');
[Knstm(4,1),Knstm(4,2),Knstm(4,3),Knstm(4,4),Knstm(4,5)]=zwfun('41','hole');
[Knstm(5,1),Knstm(5,2),Knstm(5,3),Knstm(5,4),Knstm(5,5)]=zwfun('42','hole');
[Knstm(6,1),Knstm(6,2),Knstm(6,3),Knstm(6,4),Knstm(6,5)]=zwfun('43','hole');
%The numerical integration step size
deltaz=1.6e-11;
deltazm=1.6e-11; % delt=1.3e-11 top=1.49 ans=15.0168
deltaq=1e6;
toplimz=1.49;
toplimzm=1.49;
toplimq=9e9;
% d=1e9 deltaq=10e5 ans=71.3922%lige koert paa 579s    d=1e9 deltaq=10e6 ans=77.8142
%1e6 1e8 gav 68.95meV lidt mindre end 1e9
```

```matlab
%1e5 1e8 gav 68.27meV
%5e5 1e8 gav 68.57meV


%Okay saa fandt jeg ud af at vi ikke faar uniform konvergens grundet vi har
%skrevet Z{ii}(end) hvilket ikke svarer til toppen af intervallet, men
%derimod det stykke vi naar op til foer vi overskrider intervallet med
%deltaz. Vi er derfor noedsaget til at angive endnu en variabel der hedder
%regEnd som angiver hvor hver region slutter. %foer aendringen fik jeg
%69.0334 som resultat. Det burde gerne vaere det samme efter

%Introducing the limits of the regions.
regEndz=[-d/2-t, -d/2, d/2, d/2+t, (d/2+t)*toplimz];
regEndzm=[-d/2-t, -d/2, d/2, d/2+t, (d/2+t)*toplimzm];

%Defining vectors within these region with the desired deltaz width.
Z{1}=(toplimz*(regEndz(1))):deltaz:(regEndz(1));%Electrons
Z{2}=(regEndz(1)):deltaz:(regEndz(2));
Z{3}=(regEndz(2)):deltaz:(regEndz(3));
Z{4}=(regEndz(3)):deltaz:(regEndz(4));
Z{5}=(regEndz(4)):deltaz:((regEndz(5)));
Zm{1}=(toplimzm*(regEndzm(1))):deltazm:(regEndzm(1));%Holes
Zm{2}=(regEndzm(1)):deltazm:(regEndzm(2));
Zm{3}=(regEndzm(2)):deltazm:(regEndzm(3));
Zm{4}=(regEndzm(3)):deltazm:(regEndzm(4));
Zm{5}=(regEndzm(4)):deltazm:((regEndzm(5)));

%In order for the region borders to be obeyed and the width of each slice
%(deltaz0) of the integral to be as close to the chosen delta z as
%possible, the slices are adjusted such that an integer number of slices
%will fit within the region.
for ii=1:5
zomrkonst=round((regEndz(ii)-Z{ii}(1))/deltaz);
deltaz0(ii)=(regEndz(ii)-Z{ii}(1))/zomrkonst;
zmomrkonst=round((regEndzm(ii)-Zm{ii}(1))/deltazm);%Tager ms
deltazm0(ii)=(regEndzm(ii)-Zm{ii}(1))/zmomrkonst;%tager ms
end
%The delta's should now fit. Deltaz0 is subtracted in the toplimits
%because the riemann sum is a right sum, and the subtracting one deltaz0
%ensures that we wont get a slice to much calculated with in the right
%sums.

%nu burde deltaerne passe. De foelgende ligninger behoever ikke
%at have regEnd med. Vi traekker deltaz fra i topgraenserne, eftersom disse
%kommer til at vaere en "bjaelke for meget" i hoejresummerne.
Z{1}=(toplimz*(-d/2-t)):deltaz0(1):(-d/2-t-deltaz0(1));%Elektronernes z del
Z{2}=(-d/2-t):deltaz0(2):(-d/2-deltaz0(2));
Z{3}=(-d/2):deltaz0(3):(d/2-deltaz0(3));
Z{4}=(d/2):deltaz0(4):(d/2+t-deltaz0(4));
Z{5}=(d/2+t):deltaz0(5):(toplimz*(d/2+t)-deltaz0(5));
Zm{1}=(toplimzm*(-d/2-t)):deltazm0(1):(-d/2-t-deltazm0(1));%hullernes z del
Zm{2}=(-d/2-t):deltazm0(2):(-d/2-deltazm0(2));
Zm{3}=(-d/2):deltazm0(3):(d/2-deltazm0(3));
Zm{4}=(d/2):deltazm0(4):(d/2+t-deltazm0(4));
Zm{5}=(d/2+t):deltazm0(5):(toplimzm*(d/2+t)-deltazm0(5));

%Definition of the radial n quantum numbers for both the electron and the
%hole.
ni=0;
nim=0;
nj=0;
njm=0;


Hc=zeros(4*4,4*4);
for i=1:4
    for im=1:4
        for j=1:4
            for jm=1:4
                if ~isempty(Hc((i-1)*4+j,(im-1)*4+jm))
```

```matlab
                    fprintf('jm=%.0d j=%.0d im=%.0d i=%.0d\n',jm,j,im,i)

                    %The script need to pick out the second digit of ENele
                    %(check if this can be optimized)
                    charzfori=(char(ENele(i,2))); %Electron
                    charzforim=(char(ENele(im,2))); % Electron '
                    charzmforj=(char(ENhul(j,2))); % Hole
                    charzmforjm=(char(ENhul(jm,2))); %Hole'
                    %and the third digit
                    charzforki=(char(ENele(i,3)));
                    charzforkim=(char(ENele(im,3)));
                    charzmforkj=(char(ENele(j,3)));
                    charzmforkjm=(char(ENele(jm,3)));

                    ki=charzforki(2);
                    kim=charzforkim(2);
                    kj=charzmforkj(2);
                    kjm=charzmforkj(2);

                    %The normalization integrals of the Fock Darwin states
                    ai=(integral(@(s)(s.*s.^(2*ni).*exp(-s.^2).*mfun('L',ki,ni,s.^2).^2),0,inf)...
                        *2*pi*bscaleEle^2)^(-1/2);
                    aim=(integral(@(s)(s.*s.^(2*nim).*exp(-s.^2).*mfun('L',kim,nim,s.^2).^2),0,inf)...
                        *2*pi*bscaleEle^2)^(-1/2);
                    aj=(integral(@(s)(s.*s.^(2*nj).*exp(-s.^2).*mfun('L',kj,nj,s.^2).^2),0,inf)...
                        *2*pi*bscaleHul^2)^(-1/2);
                    ajm=(integral(@(s)(s.*s.^(2*njm).*exp(-s.^2).*mfun('L',kjm,njm,s.^2).^2),0,inf)*...
                        2*pi*bscaleHul^2)^(-1/2);


                    %initialising runsum
                    runsum=0;
                    tic;

                    %Set the value of k and l
                    kafenergi(1)=ke(Knst(str2double(charzfori(1))-1+str2double(charzfori(2)),5));
                    kafenergi(2)=ke(Knst(str2double(charzforim(1))-1+str2double(charzforim(2)),5));
                    kafenergi(3)=kh(Knstm(str2double(charzmforj(1))-1+str2double(charzmforj(2)),5));
                    kafenergi(4)=kh(Knstm(str2double(charzmforjm(1))-1+str2double(charzmforjm(2)),5));

                    lafenergi(1)=le(Knst(str2double(charzfori(1))-1+str2double(charzfori(2)),5));
                    lafenergi(2)=le(Knst(str2double(charzforim(1))-1+str2double(charzforim(2)),5));
                    lafenergi(3)=lh(Knstm(str2double(charzmforj(1))-1+str2double(charzmforj(2)),5));
                    lafenergi(4)=lh(Knstm(str2double(charzmforjm(1))-1+str2double(charzmforjm(2)),5));
%The sum over q is implemented through a for loop.
for q=0:deltaq:toplimq
    runsumzm=0;
    %Calculates the electron wavefunction in each region
        for elewf=1:5
            if elewf==1
                elez=(-1)^(str2double(charzfori(1))+1)*Knst(str2double(charzfori(1))-1+...
                    str2double(charzfori(2)),1)*exp(kafenergi(1)*Z{1});
                elezim=(-1)^(str2double(charzforim(1))+1)*Knst(str2double(charzforim(1))-1+...
                    str2double(charzforim(2)),1)*exp(kafenergi(2)*Z{1});
            elseif elewf==2
                elez=(-1)^(str2double(charzfori(1))+1)*(Knst(str2double(charzfori(1))-1+...
                    str2double(charzfori(2)),2)*sin(-lafenergi(1)*Z{2})+...
                    Knst(str2double(charzfori(1))-1+str2double(charzfori(2)),3)*...
                    cos(-lafenergi(1)*Z{2}));
                elezim=(-1)^(str2double(charzforim(1))+1)*(Knst(str2double(charzforim(1))-...
                    1+str2double(charzforim(2)),2)*sin(-lafenergi(2)*Z{2})...
                    +Knst(str2double(charzforim(1))...
                    -1+str2double(charzforim(2)),3)*cos(-lafenergi(2)*Z{2}));
            elseif elewf==3
                if charzfori(1)=='1'
                    elez=Knst(str2double(charzfori(1))-1+str2double(charzfori(2)),4)...
                        *cosh(kafenergi(1)*Z{3});
                elseif charzfori(1)=='4'
                    elez=Knst(str2double(charzfori(1))-1+str2double(charzfori(2)),4)...
                        *sinh(kafenergi(1)*Z{3});
```

```matlab
            end
            if charzforim(1)=='1'
                elezim=Knst(str2double(charzforim(1))-1+str2double(charzforim(2)),4)*...
                    cosh(kafenergi(2)*Z{3});
            elseif charzforim(1)=='4'
                elezim=Knst(str2double(charzforim(1))-1+str2double(charzforim(2)),4)*...
                    sinh(kafenergi(2)*Z{3});
            end
        elseif elewf==4
            elez=(Knst(str2double(charzfori(1))-1+str2double(charzfori(2)),2)*...
                sin(lafenergi(1)*Z{4})+Knst(str2double(charzfori(1))-1+...
                str2double(charzfori(2)),3)*cos(lafenergi(1)*Z{4}));
            elezim=(Knst(str2double(charzforim(1))-1+str2double(charzforim(2)),2)...
                *sin(lafenergi(2)*Z{4})+Knst(str2double(charzforim(1))-1+...
                str2double(charzforim(2)),3)*cos(lafenergi(2)*Z{4}));
        elseif elewf==5
            elez=Knst(str2double(charzfori(1))-1+str2double(charzfori(2)),1)*...
                exp(-kafenergi(1)*Z{5});
            elezim=Knst(str2double(charzforim(1))-1+str2double(charzforim(2)),1)*...
                exp(-kafenergi(2)*Z{5});
        end
        %and the hole wavefuntions
    for hulwf=1:5
        [zcell,zmcell]=meshgrid(Z{elewf},Zm{hulwf});%Tager ms
        if hulwf==1
            hulzm=(-1)^(str2double(charzmforj(1))+1)*Knstm(str2double(charzmforj(1))-1 ...
                +str2double(charzmforj(2)),1)*exp(kafenergi(3)*Zm{1});
            hulzmm=(-1)^(str2double(charzmforjm(1))+1)*Knstm(str2double(charzmforjm(1))- ...
                1+str2double(charzmforjm(2)),1)*exp(kafenergi(4)*Zm{1});
        elseif hulwf==2
            hulzm=(-1)^(str2double(charzmforj(1))+1)*(Knstm(str2double(charzmforj(1))-1 ...
                +str2double(charzmforj(2)),2)*sin(-lafenergi(3)*Zm{2})+Knstm(str2double(charzmforj(1))...
                -1+str2double(charzmforj(2)),3)*cos(-lafenergi(3)*Zm{2}));
            hulzmm=(-1)^(str2double(charzmforjm(1))+1)*(Knstm(str2double(charzmforjm(1))...
                -1+str2double(charzmforjm(2)),2)*sin(-lafenergi(4)*Zm{2})...
                +Knstm(str2double(charzmforjm(1))-1+str2double(charzmforjm(2)),3)*...
                cos(-lafenergi(4)*Zm{2}));
        elseif hulwf==3
            if charzmforj(1)=='1'
                hulzm=Knstm(str2double(charzmforj(1))-1+str2double(charzmforj(2)),4)...
                    *cosh(kafenergi(3)*Zm{3});
            elseif charzmforj(1)=='4'
                hulzm=Knstm(str2double(charzmforj(1))-1+str2double(charzmforj(2)),4)...
                    *sinh(kafenergi(3)*Zm{3});
            end
            if charzmforjm(1)=='1'
                hulzmm=Knstm(str2double(charzmforjm(1))-1+str2double(charzmforjm(2)),4)...
                    *cosh(kafenergi(4)*Zm{3});
            elseif charzmforjm(1)=='4'
                hulzmm=Knstm(str2double(charzmforjm(1))-1+str2double(charzmforjm(2)),4)...
                    *sinh(kafenergi(4)*Zm{3});
            end
        elseif hulwf==4
            hulzm=(Knstm(str2double(charzmforj(1))-1+str2double(charzmforj(2)),2)*...
                sin(lafenergi(3)*Zm{4})+Knstm(str2double(charzmforj(1))-1+...
                str2double(charzmforj(2)),3)...
                *cos(lafenergi(3)*Zm{4}));
            hulzmm=(Knstm(str2double(charzmforjm(1))-1+str2double(charzmforjm(2)),2)...
                *sin(lafenergi(4)*Zm{4})+Knstm(str2double(charzmforjm(1))-1+...
                str2double(charzmforjm(2)),3)...
                *cos(lafenergi(4)*Zm{4}));
        elseif hulwf==5
            hulzm=Knstm(str2double(charzmforj(1))-1+str2double(charzmforj(2)),1)...
                *exp(-kafenergi(3)*Zm{5});
            hulzmm=Knstm(str2double(charzmforjm(1))-1+str2double(charzmforjm(2)),1)...
                *exp(-kafenergi(4)*Zm{5});
        end
        %The overlap in the z direction is calculated for each
        %possible combination of region for electron and hole
        [zfun,zmfun]=meshgrid(elez.*elezim,hulzm.*hulzmm);
```

```matlab
            runsumzm=runsumzm+sum(...
                sum(...
                  zfun.*zmfun.*...
                  exp(-q.*abs(zcell-zmcell))))*deltazm0(hulwf)*deltaz0(elewf);
            end
        end
        %The complete overlap for a the given value of q summed up
    runsum=runsum+...
    integral(@(s)(s.^(1+ni+nim).*exp(-s.^2).*mfun('L',ki,ni,s.^2).*...
    mfun('L',kim,nim,s.^2).*besselj(0,q*s*bscaleEle)),0,inf,'RelTol',1,'AbsTol',1e-4)*ai*aim*bscaleEle^2 ..
    * ...
    integral(@(s)(s.^(1+nj+njm).*exp(-s.^2).*mfun('L',kj,nj,s.^2).* ...
    mfun('L',kjm,njm,s.^2).*besselj(0,q*s* bscaleHul)),0,inf,'RelTol',1,'AbsTol',1e-4)*aj*ajm*bscaleHul^2 .
     * ...
     runsumzm;
 %toc
end
toc
%The coulomb matrix hamiltonian.
Hc((i-1)*4+j,(im-1)*4+jm)=runsum*deltaq*9.11028*10^-27/12.9*6.241509*10^21;
%Den naestsidste faktor er e^2*pi/epsilon den sidste faktor regner det i meV
                end
            end
        end
    end
end
```

B.2   The "EnergiZ" function

```matlab
function [l, k, a, b, B, Bm, C, Ba, Bma, Ca, ENstolv]=EnergiZ(particle)
%Funktionen udregner det for z boelgefunktionen der er uafhaengigt af hvilken
%specifik boelgefunktion man kigger paa.
d=evalin('base','d');
t=evalin('base','t');
m0=evalin('base','m0');
hbar=evalin('base','hbar');
if strcmp(particle,'electron')
    m=0.067*m0;
    v0=400*1.602176e-22; %regner fra meV til Joule
    hbaromega=20;
elseif strcmp(particle,'hole')
    m=0.38*m0;
    v0=215*1.602176e-22; %regner fra meV til Joule
    hbaromega=3.5;
else
    error('Error: second input argument must be either ''electron'' or ''hole''','');
end

syms E A
l=symfun(sqrt(2*m*E)/hbar,E);
k=symfun(sqrt(2*m*(v0-E))/hbar,E);

M=[2*cosh(d/2*k(E)) , -sin(l(E)*d/2) , -cos(l(E)*d/2);
   0 , exp(k(E)*(d/2+t))*sin(l(E)*(d/2+t)) , exp(k(E)*(d/2+t))*cos(l(E)*(d/2+t)) ;
   0, exp(k(E)*(d/2+t))*l(E)*cos(l(E)*(d/2+t)), -exp(k(E)*(d/2+t))*l(E)*sin(l(E)*(d/2+t)) ];
Dd=det(M);
%Dernaest deklareres de andre matricer
Mc=[0 , -sin(l(E)*d/2) , -cos(l(E)*d/2);
    A , exp(k(E)*(d/2+t))*sin(l(E)*(d/2+t)) , exp(k(E)*(d/2+t))*cos(l(E)*(d/2+t)) ;
    -k(E)*A , exp(k(E)*(d/2+t))*l(E)*cos(l(E)*(d/2+t)) , -exp(k(E)*(d/2+t))*l(E)*sin(l(E)*(d/2+t))];
Mb=[2*cosh(d/2*k(E)) , 0 , -cos(l(E)*d/2);
    0 , A , exp(k(E)*(d/2+t))*cos(l(E)*(d/2+t));
    0 , -k(E)*A , -exp(k(E)*(d/2+t))*l(E)*sin(l(E)*(d/2+t))];
Mbm=[2*cosh(d/2*k(E)) , -sin(l(E)*d/2) , 0;
    0 , exp(k(E)*(d/2+t))*sin(l(E)*(d/2+t)) , A;
    0, exp(k(E)*(d/2+t))*l(E)*cos(l(E)*(d/2+t)), -k(E)*A ];
%Dette bruges i sidste ende til at faa et udtryk for konstanterne der kun
%afhaenger af energien og A. Kan vises med symvar(C) eksempelvis.
```

```matlab
C=symfun(det(Mc)/Dd,E);
B=symfun(det(Mb)/Dd,E);
Bm=symfun(det(Mbm)/Dd,E);

%Energien loeses numerisk.
lh=simplify(((2*k*sinh(k*d/2)*C+Bm*l*sin(l*d/2)))/B);
rh=(l*cos(l*d/2));
b=[];
omr=1.602176e-22;
if strcmp(particle,'electron')
    for i=1:6;
        solValue=vpasolve(rh(E)-lh(E)==0,E,i*1e-20);
    if isreal(solValue)
        temp=solValue/omr;
        index=find(abs(temp-b)<1, 1);
    if isempty(index)
        b=vpa([b temp],5);
    end
    end
    end
else
    for i=1:10; %Der skal ledes i andre omraader efter hullet.
        solValue=vpasolve(rh(E)-lh(E)==0,E,i*1e-21);
    if isreal(solValue)
        temp=solValue/omr;
        index=find(abs(temp-b)<1, 1);
    if isempty(index)
        b=vpa([b temp],5);
    end
    end
    end
end

%% Dernaest antibindende for elektronerne
Ma=[2*sinh(k(E)*d/2) , -sin(l(E)*d/2) , -cos(l(E)*d/2);
    0,exp(k(E)*(d/2+t))*sin(l(E)*(d/2+t)) , cos(l(E)*(d/2+t))*exp(k(E)*(d/2+t))
    0 , l(E)*cos(l(E)*(d/2+t))*exp(k(E)*(d/2+t)) , -l(E)*sin(l(E)*(d/2+t))*exp(k(E)*(d/2+t))];
Dda=det(Ma);
Mca=[0 , -sin(l(E)*d/2) , -cos(l(E)*d/2);
    A,exp(k(E)*(d/2+t))*sin(l(E)*(d/2+t)) , cos(l(E)*(d/2+t))*exp(k(E)*(d/2+t));
    -k(E)*A , l(E)*cos(l(E)*(d/2+t))*exp(k(E)*(d/2+t)) , -l(E)*sin(l(E)*(d/2+t))*exp(k(E)*(d/2+t))];
Mba=[2*sinh(k(E)*d/2) , 0 , -cos(l(E)*d/2);
     0,A , cos(l(E)*(d/2+t))*exp(k(E)*(d/2+t));
     0 , -k(E)*A , -l(E)*sin(l(E)*(d/2+t))*exp(k(E)*(d/2+t))];
Mbma=[2*sinh(k(E)*d/2) , -sin(l(E)*d/2) , 0 ;
    0,exp(k(E)*(d/2+t))*sin(l(E)*(d/2+t)) , A;
     0 , l(E)*cos(l(E)*(d/2+t))*exp(k(E)*(d/2+t)) , -k*A];
Ca=symfun(det(Mca)/Dda,E);
Ba=symfun(det(Mba)/Dda,E);
Bma=symfun(det(Mbma)/Dda,E);
lh=simplify((Ca*2*k*cosh(k*d/2)+Bma*l*sin(l*d/2))/Ba);
rh=simplify(l*cos(l*d/2));
a=[];
if strcmp(particle,'electron')
    for i=1:6;
        solValue=vpasolve(rh(E)-lh(E)==0,E,i*1e-20);
    if isreal(solValue)
        temp=solValue/omr;
        index=find(abs(temp-a)<1, 1);
    if isempty(index)
        a=vpa([a temp],5);
    end
    end
    end
else
    for i=1:10;
        solValue=vpasolve(rh(E)-lh(E)==0,E,i*1e-21);
    if isreal(solValue)
        temp=solValue/omr;
        index=find(abs(temp-a)<1, 1);
```

```matlab
    if isempty(index)
        a=vpa([a temp],5);
    end
    end
    end
end
%%
syms b1 b2 b3 a1 a2 a3 k0 k1 k2 k3;
bs=[11 12 13]; %symbolsk vektor - bruges til at holde styr paa kombinationerne
as=[41 42 43];
%hbaromega=20;%skal vide hvilken oscillatorfrekvens der bruges
kfc=[1 3 5 7].*hbaromega;%genererer k for constant vektoren
ks=[k0 k1 k2 k3];
%smider alle kombinationer af a og k sammen over de naeste par linjer
[AA, KA]=meshgrid(a,kfc);
[BB, KB]=meshgrid(b,kfc);
AKA=AA+KA;
BKB=BB+KB;
%det samme for de symbolske udtryk
[AS, KSA]=meshgrid(as,ks);
[BS, KSB]=meshgrid(bs,ks);
%Nu laves et saet matricer der indeholder alle energimuligheder samt
%kombinationen det har taget at opnaa dem
aEN=[AKA(:), AS(:), KSA(:)];
bEN=[BKB(:),BS(:),KSB(:)];
EN=[aEN;bEN];
ENsorted=sortrows(EN,1);
ENstolv=vpa(ENsorted(1:12,:),5);
```

B.3   The "zwfun" function

```matlab
function [Atal,Btal,Bmtal,Ctal,Ez] = zwfun(charaellerb,particle)
%Funktionen udregner de ting der er specifikke for den boelgefunktion man
%kigger paa.
d=evalin('base','d');
t=evalin('base','t');
m0=evalin('base','m0');
hbar=evalin('base','hbar');
omr=evalin('base','omr');
if strcmp(particle,'electron')
    b=evalin('base','be');
    a=evalin('base','ae');
    l=evalin('base','le');
    k=evalin('base','ke');
    B=evalin('base','Be');
    Bm=evalin('base','Bme');
    C=evalin('base','Ce');
    Ba=evalin('base','Bae');
    Bma=evalin('base','Bmae');
    Ca=evalin('base','Cae');
elseif strcmp(particle,'hole')
    b=evalin('base','bh');
    a=evalin('base','ah');
    l=evalin('base','lh');
    k=evalin('base','kh');
    B=evalin('base','Bh');
    Bm=evalin('base','Bmh');
    C=evalin('base','Ch');
    Ba=evalin('base','Bah');
    Bma=evalin('base','Bmah');
    Ca=evalin('base','Cah');
else
    error('Error: second input argument must be either ''electron'' or ''hole''','');
end
syms A z
if charaellerb(1)=='1';
    Ez=b(str2double(charaellerb(2)))*omr;
    i1=int(cosh(k(Ez)*z)^2,z,0,d/2);
```

```
    i2=int((simplify(B(Ez)/A)*sin(l(Ez)*z)+simplify(Bm(Ez)/A)*cos(l(Ez)*z))^2,z,d/2,d/2+t);
    i3=int(exp(-k(Ez)*z)^2,z,d/2+t,inf);
    clear A
    syms A
    Atal=(2*((2*simplify(C(Ez)/A))^2*i1+i2+i3))^(-1/2);
    Btal=subs(B(Ez),Atal);
    Bmtal=subs(Bm(Ez),Atal);
    Ctal=subs(C(Ez),Atal);
else
    Ez=a(str2double(charaellerb(2)))*omr;
    i1=int(sinh(k(Ez)*z)^2,z,0,d/2);
    i2=int((simplify(Ba(Ez)/A)*sin(l(Ez)*z)+simplify(Bma(Ez)/A)*cos(l(Ez)*z))^2,z,d/2,d/2+t);
    i3=int(exp(-k(Ez)*z)^2,z,d/2+t,inf);
    clear A
    syms A
    Atal=(2*((2*simplify(Ca(Ez)/A))^2*i1+i2+i3))^(-1/2);
    Btal=subs(Ba(Ez),Atal);
    Bmtal=subs(Bma(Ez),Atal);
    Ctal=subs(Ca(Ez),Atal);
end
```